Delft University of Technology

Incremental Sliding-Mode Fault-Tolerant Flight Control

Wang, Xuerui; van Kampen, Erik-jan; Chu, Qiping

Important note
To cite this publication, please use the final published version (if applicable).
Please check the document version above.

Incremental Sliding-Mode Fault-Tolerant Flight Control

Xuerui Wang,* Erik-Jan van Kampen,† and Qiping Chu‡
Delft University of Technology, 2629 HS Delft, The Netherlands

and

Peng Lu§
Hong Kong Polytechnic University, Hung Hom, Kowloon, Hong Kong, People's Republic of China

DOI: 10.2514/1.G003497

This paper proposes a novel control framework that combines the recently reformulated incremental nonlinear dynamic inversion with (higher-order) sliding-mode controllers/observers, for generic multi-input/multi-output nonlinear systems, named incremental sliding-mode control. As compared to the widely used approach that designs (higher-order) sliding-mode controllers/observers based on nonlinear dynamic inversion, the proposed incremental framework can further reduce the uncertainties while requiring less model knowledge. Because the uncertainties are reduced in the incremental framework, theoretical analyses demonstrate that the incremental sliding-mode control can passively resist a wider range of perturbations with reduced minimum possible control/observer gains. These merits are validated via numerical simulations for aircraft command tracking problems, in the presence of sudden actuator faults and structural damage.

I. Introduction

SAFETY is of paramount importance to aerospace systems. Although air transport remains the safest means of transportation, it inevitably suffers from sudden actuator faults, sensor faults, and even structural damage. These faults and damage can lead to a nonequilibrium flight accompanied with varied aerodynamic properties, changed inertia properties, new sources of uncertainties, and reduced flight control authority. Therefore, fault-tolerant control [1], which is capable of automatically tolerating faults and damage while maintaining stability and desirable performance, is highly demanded.

Fault-tolerant control systems can be classified into passive fault-tolerant control systems and active fault-tolerant control systems [1,2]. Active fault-tolerant control systems use fault detection and isolation processes to obtain the most up-to-date information of the faulty system. This knowledge is then supplied to reconfigurable mechanisms to redesign the onboard controller. By contrast, passive fault-tolerant control systems are robust enough to cope with considered faults/damage without any detection nor reconfiguration [1]. Being invariant (better than just robust) to matched uncertainties [3,4], sliding-mode control methods are widely used in passive fault-tolerant control systems [1,2,5–11]. A recent flight evaluation demonstrated the effectiveness of a model-based sliding-mode controller on solving active actuator fault-tolerant control problems [12].

A well-known obstacle for sliding-mode control applications is the chattering phenomenon, caused by high-frequency switching of the control input [13,14]. Although higher-order sliding-mode control techniques offer a continuous control signal by artificially increasing the input–output relative degree, chattering is only mitigated instead of being totally eliminated [14]. Another popular approach to alleviate chattering is using approximations of the signum function,

such as saturation and sigmoid functions. However, these approximations (and hence compromises) result in partial loss of robustness [15,16]. On account of the fact that the chattering amplitude is proportional to the magnitude of the discontinuous control, a current research focus is on adaption mechanisms for achieving the minimum possible value of the control gain [13–15,17]. In spite of the variations of gain adaption methods, the sufficient condition for enforcing a sliding motion still requires the switching gain to be larger than the uncertainty bound (for first-order sliding-mode control) or the corresponding bound for uncertainty derivatives (for higher-order sliding-mode control) [13–15,17].

Many (higher-order) sliding-mode disturbance observer designs are based on sliding-mode control techniques [18–21]. For these methods, the required switching gain for guaranteeing convergence is a monotonically increasing function of the uncertainty bound or the corresponding bound for uncertainty derivatives [18–21]. Although the observations provided by disturbance observers are always continuous, the filtering process in first-order sliding-mode disturbance observer and the integration process in super-twisting disturbance observer can only attenuate instead of totally rejecting chattering in the observations [19]. Therefore, a method that could reduce the uncertainty is fundamentally beneficial for reducing the minimum possible gains of both (higher-order) sliding-mode controllers and observers.

An intuitive approach to reduce the uncertainty is using a preliminary model-based feedback control term to roughly cancel the nonlinearities and couplings. For a nonlinear system control problem, this goal is normally fulfilled by feedback linearization, also known as nonlinear dynamic inversion (NDI) in the aerospace community [22–24]. Examples that use NDI as the baseline control are first-order sliding-mode control [4–6,10,11,16,19,25–29], higher-order sliding-mode control [30–32], sliding-mode control driven by a first-order sliding-mode disturbance observer [18–20], and sliding-mode control driven by higher-order sliding-mode disturbance observers [14,15,18–21,31–33]. However, side effects of the model-based approach are also well known. For instance, pursuing decent models for complex aerospace systems is costly and time-consuming. Model identifications and updates, which are challenging and require sufficient excitations, are also necessary in the presence of faults [24].

In view of the preceding analyses, an interesting research question emerges: is there a baseline control method that could reduce the uncertainty whilst requiring less model knowledge?

Incremental nonlinear dynamic inversion (INDI) is a sensor-based control approach, which requires less model knowledge than NDI but has enhanced robustness compared to both NDI [22,23] and NDI with model identifications [24]. Numerical simulations [22–24,34,35], quadrotor flight tests [36], and passenger aircraft flight tests [37] have

consistently demonstrated the robustness and easy implementation of this method, which makes it promising as a baseline control for inducing sliding modes. This paper follows the recently reformulated INDI in [38], which is more general and more rigorous than INDI in the previous literature [22–24,34–37]. Research questions still exist for this reformulated INDI. First of all, the property of the remaining uncertainty term after INDI feedback is unclear from the literature. Moreover, there is no explicit model and analysis for the influences of sudden (discontinuous in time) faults on INDI. What is more important is that a compensation method for further improving the robustness of INDI in perturbed circumstances is desired.

The main contribution of this paper is the hybridization of (higher-order) sliding-mode controllers/observers with the reformulated INDI for generic multi-input/multi-output nonlinear systems, named incremental sliding-mode control (INDI-SMC), which inherits the advantages and remedies the drawbacks of both methods.

A. Contributions to the Reformulated Incremental Nonlinear Dynamic Inversion

In this paper, the properties (especially the boundedness) of the remaining uncertainty term after INDI feedback will be analyzed. The influences of sudden actuator faults and structural damage on INDI will also be explicitly modeled and analyzed. The robustness enhancement that sliding modes bring to INDI will be proved and numerically verified.

B. Contributions to (Higher-Order) Sliding-Mode Control

The present paper introduces an incremental sliding-mode control framework, which reduces uncertainty while requiring less model knowledge. By virtue of the uncertainty reduction, the minimum possible control/observer gains can be reduced, which is beneficial for chattering alleviation. The advantages of inducing sliding modes based on INDI instead of NDI will be analyzed and numerically validated by aircraft fault-tolerant control problems.

This paper is organized as follows. The derivations and robustness comparisons between NDI and the reformulated INDI are presented in Sec. II. The INDI-SMC framework is proposed in Sec. III, considering the hybridizations of the reformulated INDI with (higher-order) sliding-mode controllers/observers. This INDI-SMC framework is then applied to aircraft flight-tolerant control problems in Sec. IV and compared with NDI, reformulated INDI, and NDI based sliding mode control in Sec. V. Main conclusions are drawn in Sec. VI.

II. Comparisons Between Nonlinear Dynamic Inversion and the Reformulated Incremental Nonlinear Dynamic Inversion

A. Problem Formulation

Consider a multi-input/multi-output nonlinear control-affine system described by

$$\dot{x} = f(x) + G(x)u, \qquad y = h(x) \qquad (1)$$

where $f: \mathbb{R}^n \to \mathbb{R}^n$ and $h: \mathbb{R}^n \to \mathbb{R}^m$ are smooth vector fields. G is a smooth function mapping $\mathbb{R}^n \to \mathbb{R}^{n \times m}$, whose columns are smooth vector fields. Define the vector relative degree of y with respect to u as $\rho = [\rho_1, \rho_2, \ldots, \rho_m]^T$. Assume

$$\rho = \sum_{i=1}^{m} \rho_i = n$$

then by differentiating the output, the input–output mapping of the system is given by

$$y^{(\rho)} = \alpha(x) + \mathcal{B}(x)u \qquad (2)$$

where $y^\rho = [y_1^{\rho_1}, y_2^{\rho_2}, \ldots, y_m^{\rho_m}]^T$, $\alpha(x) = [\mathcal{L}_f^{\rho_1} h_1, \mathcal{L}_f^{\rho_2} h_2, \ldots, \mathcal{L}_f^{\rho_m} h_m]^T$, $\mathcal{B}(x) \in \mathbb{R}^{m \times m}$, $\mathcal{B}_{ij} = \mathcal{L}_{g_j} \mathcal{L}_f^{\rho_i-1} h_i$, and $\mathcal{L}_f^{\rho_i} h_i$, $\mathcal{L}_{g_j} \mathcal{L}_f^{\rho_i-1} h_i$ are the corresponding Lie derivatives [16]. Assume $\det\{\mathcal{B}(x)\} \neq 0$ (before

and after faults), which yields a controllable system without control redundancy. Sensor faults are not considered in the present paper, and the reader is recommended to Ref. [39] for sensor fault detection and fault-tolerant control methods. Define $\boldsymbol{\xi}_i = [h_i, \mathcal{L}_f h_i, \ldots, \mathcal{L}_f^{\rho_i-1} h_i]^T$, $\boldsymbol{\xi} = [\boldsymbol{\xi}_1; \boldsymbol{\xi}_2; \ldots; \boldsymbol{\xi}_m]$, $i = 1, 2, \ldots, m$; the nonlinear system described by Eq. (1) can be transformed into a canonical form as

$$\dot{\boldsymbol{\xi}} = A_c \boldsymbol{\xi} + B_c[\boldsymbol{\alpha}(x) + \mathcal{B}(x)u], \qquad y = C_c \boldsymbol{\xi} \qquad (3)$$

where $A_c = \mathrm{diag}\{A_0^i\}$, $B_c = \mathrm{diag}\{B_0^i\}$, $C_c = \mathrm{diag}\{C_0^i\}$, $i = 1, 2, \ldots, m$, and (A_0^i, B_0^i, C_0^i) is a canonical form representation of a chain of ρ_i integrators. The control object is to make the output y asymptotically track a reference signal $y_r(t) = [y_{r_1}(t), y_{r_2}(t), \ldots, y_{r_m}(t)]^T$. Assume $y_{r_i}(t)$, $i = 1, 2, \ldots, m$, and its derivatives up to $y_{r_i}^{(\rho_i)}(t)$ are bounded for all t, and each $y_{r_i}^{(\rho_i)}(t)$ is continuous. Denote the reference and the tracking error vectors as

$$\mathcal{R} = \left[\mathcal{R}_1; \mathcal{R}_2; \ldots; \mathcal{R}_m\right], \qquad \mathcal{R}_i = [y_{r_i}, y_{r_i}^{(1)}, \ldots, y_{r_i}^{(\rho_i-1)}]^T,$$
$$i = 1, 2, \ldots, m, \qquad e = \boldsymbol{\xi} - \mathcal{R} \qquad (4)$$

Using Eq. (3), the error dynamics are given by

$$\dot{e} = A_c(\mathcal{R} + e) + B_c[\boldsymbol{\alpha}(x) + \mathcal{B}(x)u] - \dot{\mathcal{R}}$$
$$= A_c e + B_c\left[\boldsymbol{\alpha}(x) + \mathcal{B}(x)u - y_r^{(\rho)}\right] \qquad (5)$$

where $y_r^{(\rho)} = [y_{r_1}^{(\rho_1)}, y_{r_2}^{(\rho_2)}, \ldots, y_{r_m}^{(\rho_m)}]^T$.

B. Nonlinear Dynamic Inversion and the Reformulated Incremental Nonlinear Dynamic Inversion

The standard NDI control law for stabilizing e in Eq. (5) is designed as

$$u_{\mathrm{ndi}} = \bar{\mathcal{B}}^{-1}(x)(\nu_c - \bar{\boldsymbol{\alpha}}(x)), \qquad \nu_c = y_r^{(\rho)} - Ke \qquad (6)$$

with the gain matrix $K = \mathrm{diag}\{K_i\}$, $i = 1, 2, \ldots, m$, and $K_i = [K_{i,0}, K_{i,1}, \ldots, K_{i,\rho_i-1}]$ is designed such that $A_c - B_c K$ is Hurwitz. $\nu_c \in \mathbb{R}^m$ is called the virtual control. The nominal models $\bar{\mathcal{B}}$ and $\bar{\boldsymbol{\alpha}}$ are used by NDI, which results in the closed-loop dynamics as

$$\dot{e} = (A_c - B_c K)e + B_c \boldsymbol{\varepsilon}_{\mathrm{ndi}} \qquad (7)$$

where

$$\boldsymbol{\varepsilon}_{\mathrm{ndi}} = (\boldsymbol{\alpha} - \bar{\boldsymbol{\alpha}}) + (\mathcal{B}\bar{\mathcal{B}}^{-1} - I)(\nu_c - \bar{\boldsymbol{\alpha}}) = (\boldsymbol{\alpha} - \bar{\boldsymbol{\alpha}}) + (\mathcal{B} - \bar{\mathcal{B}})u_{\mathrm{ndi}} \qquad (8)$$

$\boldsymbol{\varepsilon}_{\mathrm{ndi}}$ is the residual cancellation error of NDI caused model uncertainties, external disturbances, faults, and damage.

Following the recently reformulated INDI [38], the incremental dynamic equation is derived by taking the first-order Taylor series expansion of Eq. (2) around the current (denoted by the subscript 0) states x_0 and control input u_0 as

$$y^{(\rho)} = \boldsymbol{\alpha}(x) + \mathcal{B}(x)u$$
$$= y_0^{(\rho)} + \mathcal{B}(x_0)\Delta u + \left.\frac{\partial[\boldsymbol{\alpha}(x) + \mathcal{B}(x)u]}{\partial x}\right|_0 \Delta x + \mathcal{O}(\Delta x^2)$$
$$\triangleq y_0^{(\rho)} + \mathcal{B}(x_0)\Delta u + \boldsymbol{\delta}(x, \Delta t) \qquad (9)$$

in which Δx and Δu represent the states and control increments in one sampling time step Δt. The incremental control law for stabilizing the error dynamics in Eq. (5) is then designed as

$$\Delta u_{\mathrm{indi}} = \bar{\mathcal{B}}^{-1}(x_0)\left(\nu_c - y_0^{(\rho)}\right), \qquad \nu_c = y_r^{(\rho)} - Ke \qquad (10)$$

where K is kept identical to the gain matrix in Eq. (6) for fair comparisons. $y_0^{(\rho)}$ is measured or estimated. The total control command for actuator is hence $u_{\mathrm{indi}} = u_{\mathrm{indi},0} + \Delta u_{\mathrm{indi}}$ [38]. Substituting Eq. (10) into Eqs. (5) and (9) results in the closed-loop dynamics as

$$\dot{e} = A_c e + B_c \left[y_0^{(\rho)} + \mathcal{B}(x_0)\left(\bar{\mathcal{B}}^{-1}(x_0)\left(\nu_c - y_0^{(\rho)} \right) \right) + \delta(x, \Delta t) - y_r^{(\rho)} \right]$$
$$= (A_c - B_c K)e + B_c \varepsilon_{\mathrm{indi}} \qquad (11)$$

with

$$\varepsilon_{\mathrm{indi}} = \delta(x, \Delta t) + (\mathcal{B}\bar{\mathcal{B}}^{-1} - I)\left(\nu_c - y_0^{(\rho)} \right)$$
$$= \delta(x, \Delta t) + (\mathcal{B} - \bar{\mathcal{B}})\Delta u_{\mathrm{indi}} \qquad (12)$$

As compared to NDI control, this INDI control is less sensitive to model mismatches because the model information of $\alpha(x)$ is not used in Eq. (10). On the other hand, the INDI control law needs the measurement or estimation of $y_0^{(\rho)}$ and u_0; this is why INDI control is referred to as a sensor-based approach [36,38].

C. Comparisons Between $\varepsilon_{\mathrm{ndi}}$ and $\varepsilon_{\mathrm{indi}}$

Referring to the stability analyses in [38], if $\varepsilon_{\mathrm{ndi/indi}}$ is bounded by $\bar{\varepsilon}_{\mathrm{ndi/indi}}$, then the tracking error in Eqs. (7) and (11) is ultimately bounded by a class $\mathcal{K}$ function of $\bar{\varepsilon}_{\mathrm{ndi/indi}}$. Even so, the control performance is inevitable impaired by $\varepsilon_{\mathrm{ndi/indi}}$.

The formulations for $\varepsilon_{\mathrm{ndi}}$ and $\varepsilon_{\mathrm{indi}}$ are presented by Eqs. (8) and (12). For the reason that INDI is a sensor-based approach, in the sense that the model information of α is obtained by measuring or estimating $y_0^{(\rho)}$ and u_0, the mismatch error $\alpha - \bar{\alpha}$ in $\varepsilon_{\mathrm{ndi}}$ is accordingly replaced by $\delta(x, \Delta t)$ in $\varepsilon_{\mathrm{indi}}$. Assume that the partial derivatives of $\alpha(x)$ and $\mathcal{B}(x)$ with respect to x of any order are bounded. Because of the continuity of x, $\lim_{\Delta t \to 0} \|\Delta x\| = 0$. Therefore, recall Eq. (9), the $\delta(x, \Delta t)$ term in $\varepsilon_{\mathrm{indi}}$ satisfies

$$\lim_{\Delta t \to 0} \|\delta(x, \Delta t)\| = 0, \qquad \forall \, x \in \mathbb{R}^n \qquad (13)$$

which means that the norm value of $\delta(x, \Delta t)$ becomes negligible for sufficiently high sampling frequency. Equation (13) also indicates that $\forall \, \bar{\delta}_\varepsilon > 0, \exists \overline{\Delta t} > 0$, s.t. for all $0 < \Delta t \le \overline{\Delta t}, \forall \, x \in \mathbb{R}^n$, $\|\delta(x, \Delta t)\| \le \bar{\delta}_\varepsilon$. In other words, there exists a Δt that guarantees the boundedness of $\delta(x, \Delta t)$. Also, this bound can be further diminished by increasing the sampling frequency. The insensitivity of INDI to $\delta(x, \Delta t)$ has been numerically verified in [22–24,34–36] and flight tested in [37]. The other terms in Eqs. (8) and (12), i.e., $(\mathcal{B} - \bar{\mathcal{B}})u_{\mathrm{ndi}}$ and $(\mathcal{B} - \bar{\mathcal{B}})\Delta u_{\mathrm{indi}}$, are caused by the multiplicative uncertainties in the $\mathcal{B}(x)$ matrix.

Theorem 1: If $\|I - \mathcal{B}\bar{\mathcal{B}}^{-1}\| \le \bar{b} < 1$, for sufficiently high sampling frequency f_s, the residual error $\varepsilon_{\mathrm{indi}}$ of INDI given by Eq. (12) is ultimately bounded.

Proof: Recall Eqs. (9), (10), and (12); the output dynamics under INDI control can also be written as $y^{(\rho)} = \nu_c + \varepsilon_{\mathrm{indi}}$. Also, at the previous time step, $y_0^{(\rho)} = \nu_{c_0} + \varepsilon_{\mathrm{indi}_0}$. Therefore, using Eq. (12), $\varepsilon_{\mathrm{indi}}$ can be rewritten as

$$\varepsilon_{\mathrm{indi}} = (\mathcal{B}\bar{\mathcal{B}}^{-1} - I)\left(\nu_c - y_0^{(\rho)} \right) + \delta$$
$$= (I - \mathcal{B}\bar{\mathcal{B}}^{-1})\varepsilon_{\mathrm{indi}_0} - (I - \mathcal{B}\bar{\mathcal{B}}^{-1})(\nu_c - \nu_{c_0}) + \delta$$
$$\triangleq E\varepsilon_{\mathrm{indi}_0} - E\Delta\nu_c + \delta \qquad (14)$$

which can be written in an recursive way as

$$\varepsilon_{\mathrm{indi}}(k) = E(k)\varepsilon_{\mathrm{indi}}(k-1) - E(k)\Delta\nu_c(k) + \delta(k) \qquad (15)$$

ν_c is designed to be continuous in time; thus, the following equation holds:

$$\lim_{\Delta t \to 0} \|\nu_c - \nu_{c_0}\| = 0, \qquad \forall \, x \in \mathbb{R}^n \qquad (16)$$

Recall Eq. (13) and the subsequent discussions; for sufficiently high sampling frequency, both $\Delta\nu_c$ and $\delta(x, \Delta t)$ are bounded. Denote their bounds as $\overline{\Delta\nu_c}$ and $\bar{\delta}$, then Eq. (15) satisfies

$$\|\varepsilon_{\mathrm{indi}}(k)\| \le (\bar{b})^k \|\varepsilon_{\mathrm{indi}}(0)\| + \sum_{j=1}^{k} (\bar{b})^{k-j+1} \|\Delta\nu_c(j)\|$$
$$+ \sum_{j=1}^{k-1} (\bar{b})^{k-j} \|\delta(j)\| + \|\delta(k)\|$$
$$\le (\bar{b})^k \|\varepsilon_{\mathrm{indi}}(0)\| + \overline{\Delta\nu_c} \sum_{j=1}^{k} (\bar{b})^{k-j+1} + \bar{\delta} \sum_{j=1}^{k-1} (\bar{b})^{k-j} + \bar{\delta}$$
$$= (\bar{b})^k \|\varepsilon_{\mathrm{indi}}(0)\| + \overline{\Delta\nu_c} \frac{\bar{b} - \bar{b}^{k+1}}{1 - \bar{b}} + \bar{\delta} \frac{1 - \bar{b}^k}{1 - \bar{b}} \qquad (17)$$

Because $\bar{b} < 1$, Eq. (17) satisfies

$$\|\varepsilon_{\mathrm{indi}}\| \le \frac{\overline{\Delta\nu_c}\bar{b} + \bar{\delta}}{1 - \bar{b}}, \qquad \text{as } k \to \infty \qquad (18)$$

In conclusion, $\varepsilon_{\mathrm{indi}}$ is bounded for all k and is ultimately bounded by

$$\frac{\overline{\Delta\nu_c}\bar{b} + \bar{\delta}}{1 - \bar{b}}$$

This completes the proof. □

The boundedness of perturbations is the precondition of many robust control techniques [4]. Theorem 1 demonstrates that a sufficiently high sampling frequency f_s and $\|I - \mathcal{B}\bar{\mathcal{B}}^{-1}\| \le \bar{b} < 1$ guarantee a bounded $\varepsilon_{\mathrm{indi}}$. $f_s = 100$ Hz is a reasonable choice for flight control, as has been verified by both simulations [22–24,34,35] and passenger aircraft flight tests [37]. Moreover, $\|I - \mathcal{B}\bar{\mathcal{B}}^{-1}\| \le \bar{b} < 1$ requires a diagonally dominant structure of $\mathcal{B}\bar{\mathcal{B}}^{-1}$, which excludes unacceptable estimations of $\mathcal{B}$ (e.g., The signs of $\mathcal{B}$ and its estimation $\bar{\mathcal{B}}$ are opposite). Similar requirements can be found in [5,6,19,26,30].

By contrast, as a function of both x, u_{ndi}, and being independent of Δt, the residual error of NDI is undetermined under the same conditions. The boundedness of $\varepsilon_{\mathrm{ndi}}$ is normally assumed for the feasibility of sliding-mode control designs [5,6,19,26]. However, it will be shown in Sec. V that, even if $\|I - \mathcal{B}\bar{\mathcal{B}}^{-1}\| \le \bar{b} < 1, \varepsilon_{\mathrm{ndi}}$ has the possibility to become unbounded in severe damage cases with limited control authority. As a consequence, the NDI based sliding-mode controllers can only deal with situations where both the boundedness of $\varepsilon_{\mathrm{ndi}}$ and $\|I - \mathcal{B}\bar{\mathcal{B}}^{-1}\| \le \bar{b} < 1$ are satisfied.

One may argue that, for some moderate fault and damage cases, $\varepsilon_{\mathrm{ndi}}$ is normally bounded. Even if this is true, by comparing $\varepsilon_{\mathrm{ndi}}$ with $\varepsilon_{\mathrm{indi}}$ under the same fault/damage circumstances, $\varepsilon_{\mathrm{indi}}$ typically has smaller bound, which can be further diminished by increasing f_s. This can be demonstrated by comparing Eq. (8) with Eq. (12), where $\|\delta(x, \Delta t)\|$ becomes negligible for sufficiently high f_s [Eq. (13)], whereas $\|\alpha - \bar{\alpha}\|$ is normally large in the presence of faults and disturbances, especially for aerospace systems. Moreover, when $u_{\mathrm{ndi}} \ne 0$, there exists an f_s such that $\|\Delta u_{\mathrm{indi}}\| < \|u_{\mathrm{ndi}}\|$. Denote $\bar{\varepsilon}_{\mathrm{ndi}} = \|\alpha - \bar{\alpha}\| + \|\mathcal{B} - \bar{\mathcal{B}}\| \|u_{\mathrm{ndi}}\| \ge \|\varepsilon_{\mathrm{ndi}}\|$, and $\bar{\varepsilon}_{\mathrm{indi}} = \|\delta(x, \Delta t)\| + \|\mathcal{B} - \bar{\mathcal{B}}\| \|\Delta u_{\mathrm{indi}}\| \ge \|\varepsilon_{\mathrm{indi}}\|$, then consequently, in the perturbed conditions that $\|\alpha - \bar{\alpha}\| \ne 0, \|\mathcal{B} - \bar{\mathcal{B}}\| \ne 0$, and $\|u_{\mathrm{ndi}}\| \ne 0$, there exists an f_s such that $\bar{\varepsilon}_{\mathrm{indi}} < \bar{\varepsilon}_{\mathrm{ndi}}$.

The smaller bound of $\varepsilon_{\mathrm{indi}}$ is a useful feature because, for many (higher-order) sliding-mode controllers/observers, the required gains for inducing sliding modes are monotonically increasing functions of

the perturbation bounds. High control/observer gains are undesirable in practice because they amplify the measurement noise, excite the unmodeled parasitic dynamics, induce chattering, threaten the actuator rate and/or position limits, and potentially lead to divergence. The advantages of the incremental framework will be further demonstrated in Sec. III.

III. Proposal of the Incremental Sliding-Mode Control Framework

This section proposes a new control approach that hybridizes the reformulated INDI with (higher-order) sliding-mode controllers/observers, defined as incremental sliding-mode control (INDI-SMC). First, the control frameworks for INDI-SMC and NDI-SMC are presented. Then it will be shown in the following subsections that a wide variety of (higher-order) sliding-mode control designs in the literature belong to the NDI-SMC framework and redesigning them in the new incremental framework is beneficial for chattering reduction and robustness enhancement.

The INDI-SMC framework is proposed as

$$\Delta u_{\text{indi-}s} = \bar{\mathcal{B}}^{-1}(x_0)\left(\nu_c + \nu_s - y_0^{(\rho)}\right) \tag{19}$$

where ν_c designed for stabilizing the unperturbed system, whereas ν_s can be designed using (higher-order) sliding-mode control/observer techniques for perturbation compensations. By contrast, control methods in the literature that are in the form of

$$u_{\text{ndi-}s} = \bar{\mathcal{B}}^{-1}(x)(\nu_c + \nu_s - \bar{\alpha}(x)) \tag{20}$$

are classified as NDI-SMC.

Design the sliding variable as $\sigma(x): \mathbb{R}^n \to \mathbb{R}^m$, and define the vector relative degree of σ with respect to u as $r = [r_1, r_2, \ldots, r_m]^T$, then the dynamics of the sliding variable σ are given by

$$\sigma^{(r)} = \alpha_\sigma(x) + \mathcal{B}_\sigma(x)u, \qquad \alpha_{\sigma_i} = \mathcal{L}_f^{r_i}\sigma_i,$$
$$\mathcal{B}_{\sigma_{ij}} = \mathcal{L}_{g_j}\mathcal{L}_f^{r_i-1}\sigma_i, \qquad i, j = 1, 2, \ldots, m \tag{21}$$

In the context of sliding-mode control, σ is designed such that, when the sliding surface $\sigma = 0$ is reached, the system obtains the desirable dynamics, in spite of uncertainties. The following subsections will show how the incremental framework can be used to enforce (higher-order) sliding modes, and its advantages as compared to the NDI-SMC framework.

A. First-Order Incremental Sliding-Mode Control

In Eq. (21), if $r_i = 1$, $i = 1, 2, \ldots, m$, control methods that achieve $\sigma = 0$ are referred to as first-order (or conventional) sliding-mode control [30,40]. To reduce the switching magnitude, many sliding-mode controllers introduce a continuous preliminary feedback component based on the equivalent control method [41]. The equivalent control is defined as the control effort needed to maintain the sliding motion on the surface and is calculated by requiring $\sigma = \dot{\sigma} = 0$ [4,41]. Recalling Eq. (21), for first-order sliding mode, $\dot{\sigma} = \alpha_\sigma(x) + \mathcal{B}_\sigma(x)u_{\text{eq}} = 0$. By dynamically inverting this nonlinear algebraic equation, the equivalent control u_{eq} is calculated by

$$u_{\text{eq}} = -\mathcal{B}_\sigma^{-1}(x)\alpha_\sigma(x) \tag{22}$$

Because u_{eq} contains uncertainties and disturbances, only the model-based nominal equivalent control $\bar{u}_{\text{eq}} = -\bar{\mathcal{B}}_\sigma^{-1}(x)\bar{\alpha}_\sigma(x)$ is available for feedback control. The most widespread first-order sliding-mode control structure is

$$u = \bar{u}_{\text{eq}} + u_s = \bar{\mathcal{B}}_\sigma^{-1}(x)(\nu_s - \bar{\alpha}_\sigma(x)) \tag{23}$$

Remark 1: Equation (23) is widely used in sliding-mode control techniques regardless of the choice of sliding surface and reaching law. For example, this control structure is adopted using integral-type sliding surfaces [6,11,19,25], linear sliding surfaces [4,10,16],

dynamic sliding manifolds [26], terminal sliding surfaces [27–29], finite reaching time continuous sliding-mode designs [5], etc.

It will be shown by an example that sliding-mode control laws designed in the form of Eq. (23) are essentially NDI-based. Because INDI is able to preserve the benefits of NDI (e.g., decoupling, linearization) while requiring reduced model knowledge, it can also be used in sliding-mode control designs. The integral sliding surface is taken as an example because of its simplicity, robustness, and design flexibility.

Design the matrix $D = \text{diag}\{D_i\}$, $D_i = [K_{i,1}, \ldots, K_{i,\rho_i-1}, 1]$, $K_0 = \text{diag}\{K_{i,0}\}$, $K_{i,0} = [K_{i,0}, 0, \ldots, 0]$, $i = 1, 2, \ldots, m$, and then design the integral-type sliding variable as

$$\sigma = De - De(t_0) - \int_0^t D(A_c - B_c K)e \, d\tau$$
$$= De - De(t_0) + \int_0^t K_0 e \, d\tau \tag{24}$$

where the K matrix is the same as used in Eqs. (6) and (10). $D(A_c - B_c K) = -K_0$ can be proved by substituting the expressions for D, K_0 into Eq. (24) and using the condition that (A_0^i, B_0^i, C_0^i) is a canonical form representation of a chain of ρ_i integrators.

Equivalently, Eq. (24) can be written as

$$\sigma_i = e_i^{(\rho_i-1)} + K_{i,\rho_i-1}e^{(\rho_i-2)} + K_{i,\rho_i-2}e^{(\rho_i-3)} + \ldots + K_{i,1}e^{(0)}$$
$$+ \int_0^t K_{i,0}e_i \, d\tau - \left(e_i^{(\rho_i-1)}(t_0) + K_{i,\rho_i-1}e^{(\rho_i-2)}(t_0)\right.$$
$$\left. + K_{i,\rho_i-2}e^{(\rho_i-3)}(t_0) + \ldots + K_{i,1}e^{(0)}(t_0)\right) \tag{25}$$

It can be seen from Eq. (25) that $\sigma(t_0) = 0$, which means that if the initial conditions are known, system dynamics initiate on the sliding surface without a reaching phase. Furthermore, $\dot{\sigma} = 0$ is equal to the desired closed-loop error dynamics as shown by

$$\dot{\sigma}_i = e_i^{(\rho_i)} + K_{i,\rho_i-1}e_i^{(\rho_i-1)} + K_{i,\rho_i-2}e_i^{(\rho_i-2)} + \ldots + K_{i,1}e_i^{(1)} + K_{i,0}e_i$$
$$= 0, \qquad i = 1, 2, \ldots, m,$$
$$\dot{\sigma} = y^{(\rho)} - y_r^{(\rho)} + Ke = 0 \tag{26}$$

In the preceding equation, $y^{(\rho)}$ contains system dynamics, and $y_r^{(\rho)}$ and Ke are known or measurable. Substituting Eq. (2) into Eq. (26), the control law designed in the form of Eq. (23) is

$$\dot{\sigma} = (\alpha(x) + \mathcal{B}(x)u) - y_r^{(\rho)} + Ke = 0$$
$$u_{\text{ndi-}s} = \bar{u}_{\text{eq}} + u_s = \bar{\mathcal{B}}^{-1}(x)\left(\nu_s - \bar{\alpha}(x) - Ke + y_r^{(\rho)}\right) \tag{27}$$

which belongs to NDI-SMC [Eq. (20)] with $\nu_c = y_r^{(\rho)} - Ke$.

By contrast, if the incremental output dynamics [Eq. (9)] are substituted into Eq. (26), then INDI-SMC [Eq. (19)] is designed as

$$\dot{\sigma} = (y_0^{(\rho)} + \mathcal{B}(x_0)\Delta u + \delta(x, \Delta t)) - y_r^{(\rho)} + Ke = 0$$
$$\Delta u_{\text{indi-}s} = \bar{\mathcal{B}}^{-1}(x_0)\left(\nu_s - y_0^{(\rho)} - Ke + y_r^{(\rho)}\right) \tag{28}$$

As an example, ν_s is designed in the classical way as

$$\nu_s = -K_s \text{sign}(\sigma)$$
$$= -[K_{s,1}\text{sign}(\sigma_1), K_{s,2}\text{sign}(\sigma_2), \ldots, K_{s,m}\text{sign}(\sigma_m)]^T \tag{29}$$

where sign represents the signum function, and the switching gains $K_{s,i} > 0$, $i = 1, 2, \ldots, m$. If the conditions in Theorem 1 are satisfied, using Eq. (12), then the time derivative of the candidate Lyapunov function $V = (1/2)\sigma^T\sigma$ under the control of Eqs. (28) and (29) is calculated by

$$\dot{V} = \boldsymbol{\sigma}^T \dot{\boldsymbol{\sigma}}$$

$$= \boldsymbol{\sigma}^T \Big[\boldsymbol{y}_0^{(\rho)} + \mathcal{B}(\boldsymbol{x}_0)\bar{\mathcal{B}}^{-1}(\boldsymbol{x}_0)\big(\boldsymbol{\nu}_s - \boldsymbol{y}_0^{(\rho)} + \boldsymbol{\nu}_c\big) + \boldsymbol{\delta}(\boldsymbol{x}, \Delta t) - \boldsymbol{\nu}_c \Big]$$

$$= \boldsymbol{\sigma}^T \Big[\boldsymbol{\delta}(\boldsymbol{x}, \Delta t) + (\mathcal{B}\bar{\mathcal{B}}^{-1} - \boldsymbol{I})\big(\boldsymbol{\nu}_c - \boldsymbol{y}_0^{(\rho)}\big) + \mathcal{B}\bar{\mathcal{B}}^{-1}\boldsymbol{\nu}_s \Big]$$

$$= \boldsymbol{\sigma}^T [\boldsymbol{\varepsilon}_{\text{indi}} - \mathcal{B}\bar{\mathcal{B}}^{-1}\boldsymbol{K}_s \text{sign}(\boldsymbol{\sigma})]$$

$$\leq \sum_{i=1}^{m} \Big(|\sigma_i||\varepsilon_{\text{indi},i}| + \bar{b}K_{s,i}|\sigma_i| - K_{s,i}|\sigma_i| \Big)$$

$$\leq -\eta \sum_{i=1}^{m} |\sigma_i| = -\eta \boldsymbol{\sigma}^T \text{sign}(\boldsymbol{\sigma}), \quad \forall K_{s,i} \geq \frac{\eta + |\varepsilon_{\text{indi},i}|}{1 - \bar{b}} \quad (30)$$

where η is a small positive constant. $\dot{V} \leq -\eta \boldsymbol{\sigma}^T \text{sign}(\boldsymbol{\sigma})$ is referred to as the η reaching law and guarantees that the sliding surface $\boldsymbol{\sigma} = \boldsymbol{0}$ is reached in finite time [6–8]. On the sliding surface, the desired error dynamics are achieved, which ensure that $\boldsymbol{e}$ converges to zero.

Reviewing the discussions in Sec. II.C, the boundedness of $\boldsymbol{\varepsilon}_{\text{ndi}}$ is undetermined even if the conditions in Theorem 1 are satisfied. For the feasibility of sliding-mode control design, assume that $\boldsymbol{\varepsilon}_{\text{ndi}}$ is bounded, then similar to the derivations in Eq. (30), NDI-SMC given by Eq. (27) guarantees the convergence of $\boldsymbol{\sigma}$, when $\boldsymbol{\nu}_s = -\boldsymbol{K}_s \text{sign}(\boldsymbol{\sigma}), \forall K_{s,i} \geq (\eta + |\varepsilon_{\text{ndi},i}|)/(1 - \bar{b})$.

Remark 2: First-order sliding-mode control that contains a model-based nominal equivalent control term is essentially NDI-based and can be correspondingly designed in the proposed incremental framework. Recall the gain requirement in Eq. (30) and the analyses in Sec. II.C; this incremental framework is able to passively resist a wider range of perturbations with reduced control gains because the boundedness condition of $\boldsymbol{\varepsilon}_{\text{indi}}$ is easier to fulfill, and there exists an f_s that makes the bound of $\boldsymbol{\varepsilon}_{\text{indi}}$ smaller than the bound of $\boldsymbol{\varepsilon}_{\text{ndi}}$ under the same perturbation circumstances.

B. Higher-Order Incremental Sliding-Mode Control

The problem of higher-order sliding-mode control is equivalent to the finite time stabilization of higher-order integrator chains with bounded nonlinear perturbations [30,42]. Because NDI is able to reduce the dynamic couplings and nonlinearities by providing a preliminary feedback term based on the nominal model, it is widely used in higher-order sliding-mode controllers [30–32].

Consider an output tracking problem for the system described by Eq. (1), and choose the sliding variable as $\boldsymbol{\sigma} = \boldsymbol{y} - \boldsymbol{y}_r$. Assume that the time derivatives of $\sigma_i, \dot{\sigma}_i, \ldots, \sigma_i^{(r_i-1)}$ are continuous functions for all $i = 1, 2, \ldots, m$, and the manifold, defined as

$$\mathcal{S}^r = \{\boldsymbol{x} | \sigma_i(\boldsymbol{x}) = \dot{\sigma}_i(\boldsymbol{x}) = \ldots = \sigma_i^{(r_i-1)}(\boldsymbol{x}) = 0, \ i = 1, 2, \ldots, m\} \quad (31)$$

and called the "rth-order sliding set" [30,43], is nonempty and locally an integral set in the Filippov sense [44], then the motion on $\mathcal{S}^r$ is called the "rth-order sliding mode" with respect to the sliding variable $\boldsymbol{\sigma}$. It is noteworthy that a rth-order sliding mode can also be established for a system with relative degree ρ less than r by manually increasing the length of the integrator chains [40]. For clarity, only $\rho = r$ will be considered in the following derivations.

Recall Eqs. (2) and (5), and define $\boldsymbol{z} = [\boldsymbol{z}_1; \boldsymbol{z}_2; \ldots; \boldsymbol{z}_m]$, $\boldsymbol{z}_i = [\sigma_i(\boldsymbol{x}), \mathcal{L}_f \sigma_i(\boldsymbol{x}), \ldots, \mathcal{L}_f^{r_i-1} \sigma_i(\boldsymbol{x})]^T$, $i = 1, 2, \ldots, m$, then the dynamics of the sliding variable $\boldsymbol{\sigma}$ are given by

$$\dot{\boldsymbol{z}} = \boldsymbol{A}_c \boldsymbol{z} + \boldsymbol{B}_c \Big[\boldsymbol{\alpha}(\boldsymbol{x}) + \mathcal{B}(\boldsymbol{x})\boldsymbol{u} - \boldsymbol{y}_r^{(\rho)} \Big], \quad \boldsymbol{\sigma}^{(r)} = \boldsymbol{y}^{(\rho)} - \boldsymbol{y}_r^{(\rho)} \quad (32)$$

To achieve the rth-order sliding mode, Defoort et al. [30] design a higher-order sliding-mode controller in the form of Eq. (20) as

$$\boldsymbol{u}_{\text{ndi-}s} = \bar{\mathcal{B}}^{-1}(\boldsymbol{x})\big(\boldsymbol{\nu}_s + \boldsymbol{\nu}_n - \bar{\boldsymbol{\alpha}}(\boldsymbol{x}) + \boldsymbol{y}_r^{(\rho)}\big) \quad (33)$$

where $\boldsymbol{\nu}_n$ is a continuous virtual control to achieve the finite time stabilization of the integrator chains [30,45]. $\boldsymbol{\nu}_c = \boldsymbol{\nu}_n + \boldsymbol{y}_r^{(\rho)}$ in Eq. (33), which is able to stabilize the unperturbed system. It is

noteworthy that the formulations for $\boldsymbol{\varepsilon}_{\text{ndi/indi}}$ [Eqs. (8) and (12)] and Theorem 1 are not constrained by the specific $\boldsymbol{\nu}_c$ design; they are valid as long as $\boldsymbol{\nu}_c$ is continuous in time.

By contrast, using the incremental output dynamics [Eq. (9)], the incremental higher-order sliding-mode control law is designed in the form of Eq. (19) as

$$\Delta \boldsymbol{u}_{\text{indi-}s} = \bar{\mathcal{B}}^{-1}(\boldsymbol{x}_0)\big(\boldsymbol{\nu}_s + \boldsymbol{\nu}_n - \boldsymbol{y}_0^{(\rho)} + \boldsymbol{y}_r^{(\rho)}\big) \quad (34)$$

The rth-order sliding mode can then be established by properly designing $\boldsymbol{\nu}_n$ and $\boldsymbol{\nu}_s$. As an example, design the augmented sliding variable as $\boldsymbol{s} = \boldsymbol{\sigma}^{(r-1)} + \boldsymbol{s}_{\text{au}}, \dot{\boldsymbol{s}}_{\text{au}} = -\boldsymbol{\nu}_n$, and design $\boldsymbol{\nu}_s$ in the classical way as $\boldsymbol{\nu}_s = -\boldsymbol{K}_h \text{sign}(\boldsymbol{s}) = -[K_{h,1}\text{sign}(s_1), K_{h,2}\text{sign}(s_2), \ldots, K_{h,m}\text{sign}(s_m)]^T$, $K_{h,i} > 0, i = 1, 2, \ldots, m$. When the conditions in Theorem 1 are satisfied, using Eq. (12), the time derivative of the candidate Lyapunov function $V_s = (1/2)\boldsymbol{s}^T \boldsymbol{s}$ is

$$\dot{V}_s = \boldsymbol{s}^T \dot{\boldsymbol{s}} = \boldsymbol{s}^T \Big[\boldsymbol{y}_0^{(\rho)} + \mathcal{B}(\boldsymbol{x}_0)\bar{\mathcal{B}}^{-1}(\boldsymbol{x}_0)\big(\boldsymbol{\nu}_s + \boldsymbol{\nu}_n - \boldsymbol{y}_0^{(\rho)} + \boldsymbol{y}_r^{(\rho)}\big)$$

$$+ \boldsymbol{\delta}(\boldsymbol{x}, \Delta t) - \boldsymbol{y}_r^{(\rho)} - \boldsymbol{\nu}_n \Big]$$

$$= \boldsymbol{s}^T \Big[\boldsymbol{\delta}(\boldsymbol{x}, \Delta t) + (\mathcal{B}\bar{\mathcal{B}}^{-1} - \boldsymbol{I})\big(\boldsymbol{\nu}_c - \boldsymbol{y}_0^{(\rho)}\big) + \mathcal{B}\bar{\mathcal{B}}^{-1}\boldsymbol{\nu}_s \Big]$$

$$= \boldsymbol{s}^T \Big[\boldsymbol{\varepsilon}_{\text{indi}} - \mathcal{B}\bar{\mathcal{B}}^{-1}\boldsymbol{K}_h \text{sign}(\boldsymbol{s}) \Big]$$

$$\leq \sum_{i=1}^{m} \Big(|s_i||\varepsilon_{\text{indi},i}| + \bar{b}K_{h,i}|s_i| - K_{h,i}|s_i| \Big)$$

$$\leq -\eta \sum_{i=1}^{m} |s_i| = -\eta \boldsymbol{s}^T \text{sign}(\boldsymbol{s}), \quad \forall K_{h,i} \geq \frac{\eta + |\varepsilon_{\text{indi},i}|}{1 - \bar{b}} \quad (35)$$

Equation (35) proves that, when $K_{h,i} \geq (\eta + |\varepsilon_{\text{indi},i}|)/(1 - \bar{b})$, the sliding surface $\boldsymbol{s} = \boldsymbol{0}$ will be reached in finite time. On the sliding surface, using the equivalent control method [41], $\boldsymbol{\sigma}^{(r)} = -\dot{\boldsymbol{s}}_{\text{au}} = \boldsymbol{\nu}_n$, which means that the system dynamics are integrator chains with $\boldsymbol{\nu}_n$ as an input. Design $\boldsymbol{\nu}_n$ using the geometric homogeneity-based method introduced in [45], then the rth-order sliding mode is established in finite time.

Analogously, assume that $\|\boldsymbol{I} - \mathcal{B}\bar{\mathcal{B}}^{-1}\| \leq \bar{b} < 1$ and $\boldsymbol{\varepsilon}_{\text{ndi}}$ is bounded, then Eq. (33) guarantees the establishment of the rth-order sliding mode in finite time when $\boldsymbol{\nu}_n$ ensures finite time convergence of integrator chains, and $\boldsymbol{\nu}_s = -\boldsymbol{K}_h \text{sign}(\boldsymbol{s}), \forall K_{h,i} \geq (\eta + |\varepsilon_{\text{ndi},i}|)/(1 - \bar{b})$.

Remark 3: In view of the gain requirement in Eq. (35), similar to the Remark 2, designing a higher-order sliding-mode controller in the incremental form enables it to passively resist a wider range of perturbations using lower control gains.

Remark 4: For simplicity, the classical $\boldsymbol{\nu}_s$ design using the signum function is adopted in the preceding derivations. To migrate the chattering effects, continuous approximations of the signum function are widely used in the literature [2,4,6–9,12,16]. Other continuous $\boldsymbol{\nu}_s$ designs such as the fast terminal sliding-mode-type reaching law [29] can also be used. In spite of the variations of $\boldsymbol{\nu}_s$ designs, the relation that larger perturbation bounds require higher control gains consistently holds.

Remark 5: The sliding-mode control gains can also be adaptive, which removes the knowledge requirement on the uncertainty bound. Many advanced adaptive sliding-mode control methods are aiming for the "as small as possible" gain to migrate the chattering effects [13–15,17]. Theoretically, the smallest gain that can enforce sliding motion is a monotonically increasing function of the perturbation bound. Because there exists an f_s such that the bound of $\boldsymbol{\varepsilon}_{\text{indi}}$ is smaller as compared to the bound of $\boldsymbol{\varepsilon}_{\text{ndi}}$, the chattering reduction benefit of the incremental framework still holds in the context of adaptive sliding-mode control.

C. First-Order Incremental Sliding-Mode Control Driven by Sliding-Mode Disturbance Observers

An increasingly popular approach is designing sliding-mode control in conjunction with sliding-mode disturbance observers,

[14,15,18–21,31–33]. The main idea is using the uncertainty observations in $\boldsymbol{\nu}_s$ such that the uncertainties are directly compensated in the framework of Eq. (20). This subsection will show the merits of the incremental framework, when a first-order disturbance observer is incorporated. Higher-order sliding-mode controllers/observers will be discussed in the next subsection.

Considering the first-order sliding variable Eq. (24) with dynamics given by Eq. (26) as an example. Massey and Shtessel [18], Hall and Shtessel [19], Besnard et al. [20], and Orr and Shtessel [21] design sliding-mode controllers driven by sliding-mode disturbance observers in the form of Eq. (20), which leads to the closed-loop dynamics as

$$
\begin{aligned}
\dot{\boldsymbol{\sigma}} = y^{(\rho)} - \boldsymbol{\nu}_c &= (\boldsymbol{\alpha}(x) + \mathcal{B}(x)\boldsymbol{u}_{\text{ndi-}s}) - \boldsymbol{\nu}_c \\
&= \boldsymbol{\nu}_s + ((\boldsymbol{\alpha} - \bar{\boldsymbol{\alpha}}) + (\mathcal{B} - \bar{\mathcal{B}})\boldsymbol{u}_{\text{ndi-}s}) \triangleq \boldsymbol{\nu}_s + \boldsymbol{\varepsilon}_{\text{ndi-}s}
\end{aligned}
\tag{36}
$$

in which $\boldsymbol{\nu}_s$ contains the perturbation observations and will be designed later. It is worth noting that the uncertainties in the control effectiveness matrix $\mathcal{B}(x)$ are not considered in [18–21], whereas they are included in the present paper.

By contrast, using the incremental framework given by Eq. (19) leads to

$$
\begin{aligned}
\dot{\boldsymbol{\sigma}} = y^{(\rho)} - \boldsymbol{\nu}_c &= \left(y_0^{(\rho)} + \mathcal{B}(x_0)\Delta\boldsymbol{u}_{\text{indi-}s} + \boldsymbol{\delta}(x, \Delta t)\right) - \boldsymbol{\nu}_c \\
&= \boldsymbol{\nu}_s + \left(\boldsymbol{\delta}(x, \Delta t) + (\mathcal{B} - \bar{\mathcal{B}})\Delta\boldsymbol{u}_{\text{indi-}s}\right) \triangleq \boldsymbol{\nu}_s + \boldsymbol{\varepsilon}_{\text{indi-}s}
\end{aligned}
\tag{37}
$$

Proposition 1: If $\|\boldsymbol{I} - \mathcal{B}\bar{\mathcal{B}}^{-1}\| \leq \bar{b} < 1$, and if $\boldsymbol{\nu}_s$ is continuous in time, for sufficiently high sampling frequency f_s, the residual error term $\boldsymbol{\varepsilon}_{\text{indi-}s}$ in Eq. (37) is ultimately bounded.

Proof: The only difference between $\boldsymbol{\varepsilon}_{\text{indi-}s}$ [Eq. (37)] and $\boldsymbol{\varepsilon}_{\text{indi}}$ [Eq. (12)] is the incorporation of $\boldsymbol{\nu}_s$. In the context of sliding-mode observer designs, $\boldsymbol{\nu}_s$ is always continuous in time. Therefore, analogous to Eq. (16) and the subsequent discussions, for sufficiently high f_s, $\Delta\boldsymbol{\nu}_s = \boldsymbol{\nu}_s - \boldsymbol{\nu}_{s_0}$ is bounded. Denote the bound as $\overline{\Delta\boldsymbol{\nu}_s}$, then analogous to the proof of Theorem 1, $\boldsymbol{\varepsilon}_{\text{indi-}s}$ is bounded for all k, and is ultimately bounded by

$$
\|\boldsymbol{\varepsilon}_{\text{indi-}s}\| \leq \frac{\overline{\Delta\boldsymbol{\nu}_c}\bar{b} + \overline{\Delta\boldsymbol{\nu}_s}\bar{b} + \bar{\delta}}{1 - \bar{b}}
\tag{38}
$$

This completes the proof. □

Moreover, because $\boldsymbol{\nu}_s$ is continuous in time, similar to the discussions in Sec. II.C, under the same perturbation circumstances, there exists an f_s such that $\boldsymbol{\varepsilon}_{\text{indi-}s}$ has a smaller bound as compared to $\boldsymbol{\varepsilon}_{\text{ndi-}s}$ [Eq. (36)]. This feature is beneficial for disturbance observations, which will be shown as follows.

Using the first-order sliding-mode disturbance observer proposed in [18–21], the auxiliary sliding variable s is designed as $s = \boldsymbol{\sigma} + z_o$, $\dot{z}_o = -\boldsymbol{\nu}_s - \boldsymbol{\nu}_o$, with dynamics $\dot{s} = \boldsymbol{\varepsilon}_{\text{ndi-}s/\text{indi-}s} - \boldsymbol{\nu}_o$ under the control of Eqs. (20) and (19). If s is stabilized by $\boldsymbol{\nu}_o = K_{ob}\text{sign}(s)$, then the equivalent control exactly equals $\boldsymbol{\varepsilon}_{\text{ndi-}s/\text{indi-}s}$. This equivalent control can be estimated by low-pass filtering $\boldsymbol{\nu}_o$; consequently, the estimated equivalent control $\hat{\boldsymbol{\nu}}_{\text{eq}}$ reconstructs $\boldsymbol{\varepsilon}_{\text{ndi-}s/\text{indi-}s}$ with a small error proportional to the time constant of the low-pass filter. Finally, designing $\boldsymbol{\nu}_s = -K_\sigma\boldsymbol{\sigma} - \hat{\boldsymbol{\nu}}_{\text{eq}}$ with positive-definite K_σ ensures that $\boldsymbol{\sigma}$ is bounded by an arbitrarily small bound.

Remark 6: The sufficient condition for stabilizing s is the observer gains $K_{ob,i} > |\boldsymbol{\varepsilon}_{\text{ndi-}s/\text{indi-}s,i}| + \eta$, with a small positive η. Even though the observation term $\boldsymbol{\nu}_s$ is continuous, the chattering effects are only attenuated instead of being rejected by the filtering process [19]. Therefore, aiming for the "as small as possible" observer gains is still meaningful. Because there exists an f_s such that $\boldsymbol{\varepsilon}_{\text{indi-}s}$ has a smaller bound as compared to $\boldsymbol{\varepsilon}_{\text{ndi-}s}$, the incremental framework is beneficial for chattering reduction.

D. Higher-Order Incremental Sliding-Mode Control Driven by Sliding-Mode Disturbance Observers

This subsection will show how to design a higher-order sliding-mode control driven by a higher-order sliding-mode disturbance observer in the incremental framework. Following the derivations in Sec. III.B, design the sliding variable as $\boldsymbol{\sigma} = y - y_r$ and design $\boldsymbol{\nu}_c = \boldsymbol{\nu}_n + y_r^{(\rho)}$, then the dynamics of $\boldsymbol{\sigma}$ under the control of Eq. (20) is

$$
\begin{aligned}
\boldsymbol{\sigma}^{(r)} = y^{(\rho)} - y_r^{(\rho)} &= \bar{\boldsymbol{\alpha}}(x) + \bar{\mathcal{B}}(x)\boldsymbol{u}_{\text{ndi-}s} + \boldsymbol{\varepsilon}_{\text{ndi-}s} - y_r^{(\rho)} \\
&= \boldsymbol{\nu}_n + \boldsymbol{\nu}_s + \boldsymbol{\varepsilon}_{\text{ndi-}s}
\end{aligned}
\tag{39}
$$

By contrast, using Eqs. (9) and (37), the dynamics of $\boldsymbol{\sigma}$ under the control of Eq. (19) equals

$$
\begin{aligned}
\boldsymbol{\sigma}^{(r)} = y^{(\rho)} - y_r^{(\rho)} &= y_0^{(\rho)} + \bar{\mathcal{B}}(x_0)\Delta\boldsymbol{u}_{\text{indi-}s} + \boldsymbol{\varepsilon}_{\text{indi-}s} - y_r^{(\rho)} \\
&= \boldsymbol{\nu}_n + \boldsymbol{\nu}_s + \boldsymbol{\varepsilon}_{\text{indi-}s}
\end{aligned}
\tag{40}
$$

The only difference between Eqs. (39) and (40) is the value of the perturbation terms. Because $\boldsymbol{\varepsilon}_{\text{indi-}s}$ has better properties than $\boldsymbol{\varepsilon}_{\text{ndi-}s}$, higher-order sliding-mode disturbance observers, such as the (adaptive) super-twisting disturbance observer, designed for Eq. (39) [14,15,18–21,31–33] can be straightforwardly applied to Eq. (40). Design the augmented sliding variable as $s = \boldsymbol{\sigma}^{(r-1)} + s_{\text{au}}$, $\dot{s}_{\text{au}} = -\boldsymbol{\nu}_n$, then $\dot{s} = \boldsymbol{\nu}_s + \boldsymbol{\varepsilon}_{\text{ndi-}s/\text{indi-}s}$ for dynamics given by Eqs. (39) and (40). If s is stabilized by the (adaptive) supertwisting control, then $\boldsymbol{\nu}_s$ observes $-\boldsymbol{\varepsilon}_{\text{ndi-}s/\text{indi-}s}$ in finite time. Consequently, the closed-loop systems described by Eqs. (39) and (40) behave like unperturbed systems in finite time. It is noteworthy that the observation term $\boldsymbol{\nu}_s$ provided by (adaptive) super-twisting observer is continuous because of the integration of the signum function.

Remark 7: Theoretically, an (adaptive) super-twisting control/ observer may be less suitable for resisting sudden (discontinuous in time) onboard faults or damage because the classical supertwisting control/observer requires bounded $\dot{\boldsymbol{\varepsilon}}_{\text{ndi-}s/\text{indi-}s}$, and the adaptive supertwisting requires bounded $\ddot{\boldsymbol{\varepsilon}}_{\text{ndi-}s/\text{indi-}s}$ [14,15,19]. Nevertheless, many physical processes in reality are at least twice differentiable, which makes the incorporation of (adaptive) supertwisting control/ observer possible.

E. Advantages of the Incremental Sliding-Mode Control Framework

In this subsection, the NDI [Eq. (6)], INDI [Eq. (10)], NDI-SMC [Eq. (20)], and INDI-SMC [Eq. (19)] methods will be compared. The main focus of this paper is demonstrating the properties of the incremental framework, instead of specific $\boldsymbol{\nu}_c$ and $\boldsymbol{\nu}_s$ designs. Therefore, the following comparisons are also independent of $\boldsymbol{\nu}_c, \boldsymbol{\nu}_s$, as long as they are kept consistent in the four different control frameworks for fair comparisons.

Figure 1 illustrates the relations of the four control frameworks. When the sliding-mode module for calculating $\boldsymbol{\nu}_s$ is deactivated, Fig. 1 shows the control structure of NDI and INDI. To be specific, when the two switches are connected with the blue dashed lines, Fig. 1 shows the control structure of NDI, where the nominal model $\bar{\boldsymbol{\alpha}}(x)$ is needed. By contrast, when the two switches are connected with the back solid lines, Fig. 1 shows the control structure of INDI. As can be seen from Fig. 1, INDI does not need the model $\bar{\boldsymbol{\alpha}}(x)$ but requires the measurements/estimations of $y_0^{(\rho)}$ and $\boldsymbol{u}_{\text{indi},0}$. Activating the sliding-mode module inserts the $\boldsymbol{\nu}_s$ virtual control for resisting perturbations, which results in the NDI-SMC and INDI-SMC frameworks. Moreover, INDI and INDI-SMC design the control increments, whereas NDI and NDI-SMC directly design the total control commands.

By virtue of the incorporation of $\boldsymbol{\nu}_s$, the advantage of INDI-SMC over INDI is straightforward (i.e., robustness enhancement). On the other hand, the advantages of the INDI-SMC framework over NDI-SMC are 1) less model dependency and lower computational burden, 2) lower sliding-mode control/observer gains required, 3) improved robustness because INDI is more robust than NDI, and 4) capability to solve problems that are nonaffine in the control.
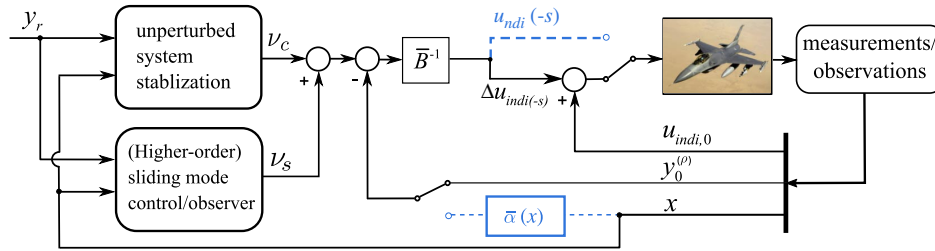
Fig. 1   Control structures of NDI, INDI, NDI-SMC, and INDI-SMC.

$\bar{\boldsymbol{\alpha}}(\boldsymbol{x})$ contains the aerodynamics for aerospace systems, which are difficult to be modeled accurately. Because the incremental framework is independent of $\bar{\boldsymbol{\alpha}}(\boldsymbol{x})$, the implementation process is simplified, and the computational burden can also be reduced. INDI-SMC also requires lower control and observer gains, mainly because of the better properties of $\boldsymbol{\varepsilon}_{\text{indi}(-s)}$. As proved by Theorem 1 and Proposition 1, sufficiently high f_s and a diagonally dominant structure of $\mathcal{B}\bar{\mathcal{B}}^{-1}$ ensure the boundedness of $\boldsymbol{\varepsilon}_{\text{indi}(-s)}$, whereas the boundedness of $\boldsymbol{\varepsilon}_{\text{ndi}(-s)}$ is not guaranteed under the same conditions. Moreover, in the same fault scenario, there exists an f_s such that $\boldsymbol{\varepsilon}_{\text{indi}(-s)}$ has a smaller bound as compared to $\boldsymbol{\varepsilon}_{\text{ndi}(-s)}$. These properties enable INDI-SMC to passively resist a wider range of perturbations using lower control and observer gains, as compared to NDI-SMC in the literature. In addition, the incremental framework can also deal with nonaffine in the control problems because the incremental dynamic equation [Eq. (9)] is derived by taking partial derivative with respect to $\boldsymbol{u}$. The merits of the incremental sliding-mode control framework will be numerically verified in Sec. V.

IV.   Fault-Tolerant Flight Control Design

In this section, the nominal six-degree-of-freedom nonlinear equations of motion of aircraft are given first. Then the actuator faults and structural damage are modeled. After that, the control methods derived in Sec. III are applied to aircraft fault-tolerant control problems.

A.   Nominal Equations of Motion

In the nominal case, the origin of the body-fixed frame is assumed to coincide with the aircraft center of mass (c.m.), and the equations of motion for a rigid aircraft are given by

$$\begin{bmatrix} \dot{\boldsymbol{V}} \\ \dot{\boldsymbol{\omega}} \end{bmatrix} = \begin{bmatrix} m\boldsymbol{I} & \boldsymbol{0} \\ \boldsymbol{0} & \boldsymbol{J} \end{bmatrix}^{-1} \begin{bmatrix} -m\tilde{\boldsymbol{\omega}}\boldsymbol{V} + \boldsymbol{F} \\ -\tilde{\boldsymbol{\omega}}\boldsymbol{J}\boldsymbol{\omega} + \boldsymbol{M} \end{bmatrix}$$
$$\dot{\boldsymbol{\theta}} = \boldsymbol{T}(\boldsymbol{\theta})\boldsymbol{\omega} \tag{41}$$

where $\boldsymbol{V} = [u, v, w]^T$ and $\boldsymbol{\omega} = [p, q, r]^T$ represent the translation and rotational velocities of the body-fixed frame relative to the inertial frame. $\boldsymbol{\theta} = [\phi, \theta, \psi]^T$ contains the Euler angles. m is the total mass, and $\boldsymbol{J}$ represents the inertia matrix. $\boldsymbol{F}$ and $\boldsymbol{M}$ are the total force and moment vectors. The $\boldsymbol{T}(\boldsymbol{\theta})$ matrix links angular velocities $\boldsymbol{\omega}$ to Eulerian velocities $\dot{\boldsymbol{\theta}}$. Bold mark indicates vectors and matrices. $(\tilde{\cdot})$ denotes the skew-symmetric matrix of the corresponding vector. $\boldsymbol{F}$ and $\boldsymbol{M}$ contain aerodynamic, gravitational, and thrust forces and moments. Furthermore, the aerodynamic forces and moments are normally given as functions of the aerodynamic coefficients as

$$\boldsymbol{M}_a = q_\infty S \text{diag}([b, \bar{c}, b]) \left(\begin{bmatrix} C_l(\beta, r, p) \\ C_m(\alpha, \dot{\alpha}, q) \\ C_n(\beta, r, p) \end{bmatrix} \right.$$
$$\left. + \begin{bmatrix} C_{l_{\delta_a}}(\alpha, \beta) & 0 & C_{l_{\delta_r}}(\alpha, \beta) \\ 0 & C_{m_{\delta_e}}(\alpha) & 0 \\ C_{n_{\delta_a}}(\alpha, \beta) & 0 & C_{n_{\delta_r}}(\alpha, \beta) \end{bmatrix} \begin{bmatrix} \delta_a \\ \delta_e \\ \delta_r \end{bmatrix} \right)$$
$$\boldsymbol{F}_a = q_\infty S \big[C_x(\alpha, \beta, q, \delta_e), C_y(\alpha, \beta, p, r, \delta_a, \delta_r), C_z(\alpha, \beta, q, \delta_e) \big]^T \tag{42}$$

In the preceding equation, α, β represent the angle of attack and the sideslip angle. V is the airspeed, and the dynamic pressure is given by $q_\infty = 0.5\rho V^2$ (ρ is the air density). S, b, $\bar{c}$ are the wing area, wing span, and mean aerodynamic chord, respectively.

B.   Actuator Faults

The actuator faults considered in this paper are the loss of control surface area and control surface jamming problems. The inertia effects of loss of control surface area are assumed to be negligible, and the aerodynamic effects can be modeled by multiplying the control derivatives with an effectiveness scaling factor, namely, $C'_{i_j} = \mu_j C_{i_j}$, $i = l, m, n$, $j = \delta_a, \delta_e, \delta_r$, $\mu_j \in [0, 1]$, with the prime symbol indicating the postfailure condition.

There are two main effects of actuator jamming. One is the influence on control effectiveness, and the other is the induced extra forces and moments. If one side of the ailerons or elevators is stuck, the corresponding control derivatives are halved (i.e., $\mu_j = 0.5$, $j = \delta_a, \delta_e$). Jamming faults also introduce new control derivatives such that the decoupling between longitudinal and lateral controls no longer holds. Specifically, aileron jamming would introduce $C_{m_{\delta_a}}$, and elevator jamming would introduce $C_{l_{\delta_e}}$ and $C_{n_{\delta_e}}$.

Furthermore, extra forces and moments will be induced if control surfaces are jammed at nonneutral positions. If one of the ailerons is jammed at $\delta_{a\Delta}$, the induced force and moment coefficients can be given by

$$\Delta C_l = \frac{1}{2} C_{l_{\delta_a}} \delta_{a\Delta}, \qquad \Delta C_n = \frac{1}{2} C_{n_{\delta_a}} \delta_{a\Delta}, \qquad \Delta C_y = \frac{1}{2} C_{y_{\delta_a}} \delta_{a\Delta},$$
$$\Delta C_z = \frac{\Delta C_l b}{r_{a_y}}, \qquad \Delta C_m = -\frac{\Delta C_l b r_{a_x}}{\bar{c} r_{a_y}} \tag{43}$$

where $\boldsymbol{r}_a = [r_{a_x}, r_{a_y}, r_{a_z}]^T$ is the position vector from the c.m. to the aerodynamic center of the jammed aileron. Analogously, the induced force and moment coefficients of one-side elevator jamming is calculated by

$$\Delta C_z = -\frac{C_{m_{\delta_e}} \delta_{e\Delta} \bar{c}}{2r_{e_x}}, \quad \Delta C_m = \frac{1}{2} C_{m_{\delta_e}} \delta_{e\Delta}, \quad \Delta C_l = \frac{\Delta C_z r_{e_y}}{b} \tag{44}$$

where $\boldsymbol{r}_e = [r_{e_x}, r_{e_y}, r_{e_z}]^T$ indicates the position vector from the c.m. to the aerodynamic center of the jammed elevator.

C.   Structural Damage

There are three main effects of structural damage: the changes of aerodynamic properties, inertia properties, and the control effectiveness [46,47].

Structural damage may reduce the control effectiveness and introduce new control derivatives if asymmetric damage is encountered. The methods for modeling these effects have been discussed in the previous subsection.

Structural damage is normally accompanied with mass loss. As a consequence, the center of mass instantaneously shifts to a new location. Because Eq. (41) uses the c.m. as the reference frame origin O, it should be modified for postdamage cases.

A conventional way to model the dynamics of postdamage aircraft is setting up the equations of motion (EoM) on the new c.m. location O', which is referred to as the c.m.-centric method in [47]. Denote the

distance vector from O to O' as $\boldsymbol{r}_{OO'} = [r_{\Delta x}, r_{\Delta y}, r_{\Delta z}]^T$. When using the c.m.-centric method, Eq. (41) can still be used for postdamage conditions. Consequently, the reference point of moments due to external forces should be transferred to the new c.m. location O'. Furthermore, the inertia tensor needs to be modified with respect to the new point O' using the parallel axis theorem. Last but not least, the translational velocity V in Eq. (41) actually refers to the velocity of a new point O', with the relationship $\boldsymbol{V}_{O'} = \boldsymbol{V}_O + \boldsymbol{\omega} \times \boldsymbol{r}_{OO'}$. As a result, there is a discontinuity in V if $\boldsymbol{\omega}$ is nonzero at the damage instant, and so a trigger logic to reset the integrator of V is required. This discontinuity and trigger logic are totally avoided by using the non-c.m. approach [47], which means that the frame origin is still fixed on O after damage. The reference frames for moments and inertia tensor are also kept invariant. Additionally, the moment due to gravity $\boldsymbol{M}_G = \boldsymbol{r}_{OO'} \times \boldsymbol{G}$ needs to be added. The equations of motion using the non-c.m. approach are given by [35,47]

$$\begin{bmatrix} \dot{\boldsymbol{V}} \\ \dot{\boldsymbol{\omega}} \end{bmatrix} = \begin{bmatrix} m'\boldsymbol{I} & \tilde{\boldsymbol{S}}^T \\ \tilde{\boldsymbol{S}} & \boldsymbol{J}' \end{bmatrix}^{-1} \begin{bmatrix} -m'\tilde{\boldsymbol{\omega}}\boldsymbol{V} - \tilde{\boldsymbol{\omega}}\tilde{\boldsymbol{S}}^T\boldsymbol{\omega} + \boldsymbol{F}' \\ -\tilde{\boldsymbol{V}}\tilde{\boldsymbol{S}}^T\boldsymbol{\omega} - \tilde{\boldsymbol{\omega}}\,\tilde{\boldsymbol{S}}\,\boldsymbol{V} - \tilde{\boldsymbol{\omega}}\boldsymbol{J}'\boldsymbol{\omega} + \boldsymbol{M}' \end{bmatrix} \quad (45)$$

The tilde symbol in Eq. (45) denotes the corresponding skew-symmetric matrix of the vector. $\boldsymbol{S} = [m'r_{\Delta x}, m'r_{\Delta y}, m'r_{\Delta z}]^T$ is nonzero when using the non-c.m. approach, which leads to coupled translational and rotational motions.

The aerodynamic characteristics of partially damaged aircraft have been investigated in [46,48]. It has been found that damage of horizontal stabilizers leads to significant loss in both static and dynamic longitudinal stability. The static derivative C_{m_α} and damping derivative C_{m_q} are approximately linear to the scale of tip loss. An additional rolling moment coefficient due to pitch rate ΔC_{l_q} is induced if geometric asymmetrical damage is imposed on horizontal stabilizers.

Similarly, damage of the vertical tail causes reductions in static and dynamic stability on the directional axis with an approximately linear relationship with the damage scale. These effects are reflected by reductions of C_{n_β} and C_{n_r}.

The tip loss of the wing directly leads to the reduction of the lift slope C_{L_α}. The unequal lift on left and right wings also induces an additional rolling moment coefficient $\Delta C_l(\alpha)$. For aircraft with positive dihedral angle, C_{l_β} reduces as the wing area decreases. The rolling damping coefficient C_{l_p} is also expected to reduce because the wing is the major source of rolling damping. Similar to the effects of asymmetric horizontal stabilizer damage, the asymmetric wing damage would also generate a rolling moment coefficient during pitch motions indicated by ΔC_{l_q}.

The influences of wing, horizontal stabilizer, and vertical tail damage on aerodynamic coefficients are summarized in Table 1.

D. Aircraft Attitude Fault-Tolerant Control Design

Recall Eqs. (41) and (42). The aircraft attitude dynamics can be written in a more compact form as

$$\dot{\boldsymbol{x}}_1 = \boldsymbol{f}_1(\boldsymbol{x}_1)\boldsymbol{x}_2$$
$$\dot{\boldsymbol{x}}_2 = \boldsymbol{f}_2(\boldsymbol{x}_1, \boldsymbol{x}_2) + \boldsymbol{G}_2\boldsymbol{u} \quad (46)$$

where $\boldsymbol{x}_1 = [\phi, \theta, \psi]^T$, $\boldsymbol{x}_2 = [p, q, r]^T$, and $\boldsymbol{u} = [\delta_a, \delta_e, \delta_r]^T$. The plant is perturbed by model uncertainties, damage, and failures:

$$\boldsymbol{f}_2 = \bar{\boldsymbol{f}}_2 + (\boldsymbol{f}_{f_2} - \bar{\boldsymbol{f}}_2)\kappa + \Delta\boldsymbol{f}_2, \quad \boldsymbol{G}_2 = \bar{\boldsymbol{G}}_2 + (\boldsymbol{G}_{f_2} - \bar{\boldsymbol{G}}_2)\kappa + \Delta\boldsymbol{G}_2 \quad (47)$$

Table 1 The main influences of structural damage on aerodynamic coefficients

Damaged component	Changed coefficients	New coefficients
Horizontal stabilizer	C_{m_α}, C_{m_q}	ΔC_{l_q}
Vertical tail	C_{n_β}, C_{n_r}	—
Wing	$C_{L_\alpha}, C_{l_\beta}, C_{l_p}$	$\Delta C_{l_q}, \Delta C_l(\alpha)$

In Eq. (47), $\bar{\boldsymbol{f}}_2$ and $\bar{\boldsymbol{G}}_2$ represent the nominal dynamics given by Eq. (41). $\boldsymbol{f}_{f_2}$ and $\boldsymbol{G}_{f_2}$ denote the new dynamics after sudden actuator faults or structural damage. $\Delta\boldsymbol{f}_2$ and $\Delta\boldsymbol{G}_2$ indicate the model uncertainty terms as continuous functions of $\boldsymbol{x}$. $\kappa(t) \in [0, 1]$ is a failure indicator, where $\kappa = 1$ denotes postfault condition, and $\kappa = 0$ denotes the fault-free case. $\kappa(t)$ is designed as a unit step function to indicate the sudden structure breaks and actuator faults during flight. Because the first equation of Eq. (46) represents the kinematics of the aircraft attitude, there is no model uncertainty ($\boldsymbol{f}_1 = \bar{\boldsymbol{f}}_1$). V, α, β in Eq. (42) are viewed as measurable inputs. Choosing $\boldsymbol{y} = \boldsymbol{x}_1$, the vector relative degree is then $\boldsymbol{\rho} = [2, 2, 2]^T$. With knowledge only about the nominal model, the controller aims at passively tolerating these faults/damage and model uncertainties. This paper chooses the attitude control as a demonstrative case for testing the decoupling performance of the controllers. The output and $\boldsymbol{x}_1$ can also be chosen as $\boldsymbol{y} = \boldsymbol{x}_1 = [\mu, \alpha, \beta]^T$ or $\boldsymbol{y} = \boldsymbol{x}_1 = [\phi, \theta, \beta]^T$. Using the kinematic equations for μ, α, β [24], the vector relative degree for these two choices still equals $\boldsymbol{\rho} = [2, 2, 2]^T$. Therefore, the control methods designed in this paper can be applied straightforwardly.

Using Eqs. (8) and (46), the NDI control input is $\boldsymbol{u}_{\mathrm{ndi}} = \bar{\mathcal{B}}^{-1}(\boldsymbol{\nu}_c - \bar{\boldsymbol{\alpha}})$ [Eq. (6)] with residual error

$$\boldsymbol{\varepsilon}_{\mathrm{ndi}} = (\boldsymbol{\alpha} - \bar{\boldsymbol{\alpha}}) + (\mathcal{B}\bar{\mathcal{B}}^{-1} - \boldsymbol{I})(\boldsymbol{\nu}_c - \bar{\boldsymbol{\alpha}})$$
$$= \boldsymbol{f}_1(\boldsymbol{f}_2 - \bar{\boldsymbol{f}}_2) + (\boldsymbol{f}_1\boldsymbol{G}_2\bar{\boldsymbol{G}}_2^{-1}\boldsymbol{f}_1 - \boldsymbol{I})\left(\boldsymbol{\nu}_c - \frac{\partial\boldsymbol{f}_1\boldsymbol{x}_2}{\partial\boldsymbol{x}_1}(\boldsymbol{f}_1\boldsymbol{x}_2) - \boldsymbol{f}_1\bar{\boldsymbol{f}}_2\right) \quad (48)$$

where $\boldsymbol{f}_1 = \bar{\boldsymbol{f}}_1$ is used in the preceding equation. The INDI controller is designed by Eq. (10), but because a new variable κ as a discontinuous function of time is incorporated to indicate the sudden faults/damage onboard, $\boldsymbol{\delta}(\boldsymbol{x}, \Delta t)$ in Eq. (9) needs to be augmented by a $\Delta\kappa$ related term as

$$\boldsymbol{\delta}'(\boldsymbol{x}, \Delta\kappa, \Delta t) \triangleq \boldsymbol{\delta}(\boldsymbol{x}, \Delta t) + \boldsymbol{\eta}_\kappa$$
$$= \left[\frac{\partial[\boldsymbol{\alpha} + \mathcal{B}\boldsymbol{u}]}{\partial\boldsymbol{x}}\bigg|_0 \Delta\boldsymbol{x} + \mathcal{O}(\Delta\boldsymbol{x}^2)\right] + \frac{\partial[\boldsymbol{\alpha} + \mathcal{B}\boldsymbol{u}]}{\partial\kappa}\bigg|_0 \Delta\kappa \quad (49)$$

Using Eqs. (46) and (47), $\boldsymbol{\eta}_\kappa$ is calculated as

$$\boldsymbol{\eta}_\kappa = \frac{\partial[(\partial\boldsymbol{f}_1\boldsymbol{x}_2/\partial\boldsymbol{x}_1)(\boldsymbol{f}_1\boldsymbol{x}_2) + \boldsymbol{f}_1\boldsymbol{f}_2 + \boldsymbol{f}_1\boldsymbol{G}_2\boldsymbol{u}]}{\partial\kappa}\bigg|_0 \Delta\kappa$$
$$= \boldsymbol{f}_1\Big[(\boldsymbol{f}_{f_2} - \bar{\boldsymbol{f}}_2) + (\boldsymbol{G}_{f_2} - \bar{\boldsymbol{G}}_2)\boldsymbol{u}\Big]\bigg|_0 \Delta\kappa \quad (50)$$

Because $\kappa(t)$ is a unit step function, $\Delta\kappa(t)$ is a single square pulse with magnitude of 1 and width of Δt. Consequently, this $\boldsymbol{\eta}_\kappa$ term is only nonzero at the failure instant, and at the next time step, the faults/damage have already been reflected in the measurements. This remarkable feature makes the sensor-based INDI a promising approach for fault-tolerant control problems.

Recalling Eq. (50), $\boldsymbol{\eta}_\kappa$ is bounded if, at the fault instant t_f, $[(\boldsymbol{f}_{f_2} - \bar{\boldsymbol{f}}_2) + (\boldsymbol{G}_{f_2} - \bar{\boldsymbol{G}}_2)\boldsymbol{u}]|_{t=t_f}$ is bounded. This is a reasonable assumption because more strict requirements on the boundedness of $\boldsymbol{f}_2 - \bar{\boldsymbol{f}}_2 = (\boldsymbol{f}_{f_2} - \bar{\boldsymbol{f}}_2)\kappa + \Delta\boldsymbol{f}_2$ and $\boldsymbol{G}_2 - \bar{\boldsymbol{G}}_2 = (\boldsymbol{G}_{f_2} - \bar{\boldsymbol{G}}_2)\kappa + \Delta\boldsymbol{G}_2$ for all t are often made in the literature [2,5–10]. Denote the bound of $\boldsymbol{\eta}_\kappa$ as $\bar{\eta}_\kappa$; recalling Eq. (49), $\|\boldsymbol{\delta}'(\boldsymbol{x}, \Delta\kappa, \Delta t)\| \leq \|\boldsymbol{\delta}(\boldsymbol{x}, \Delta t)\| + \bar{\eta}_\kappa$. As a result, Theorem 1 and Proposition 1 are valid when κ is involved. Furthermore, because $\boldsymbol{\eta}_\kappa$ converges to zero after the fault occurs, the ultimate bound of $\boldsymbol{\varepsilon}_{\mathrm{indi(-s)}}$ is not influenced by $\bar{\eta}_\kappa$. Even though this $\boldsymbol{\eta}_\kappa$ term only appears at the fault/damage instant, it inevitably degrades the tracking performance of INDI. Therefore, it is meaningful to incorporate $\boldsymbol{\nu}_s$ into INDI for robustness enhancement.

V. Numerical Validation

In this section, the NDI, INDI, NDI-SMC, and INDI-SMC designed for an aircraft command tracking problem will be compared

Table 2   Limits and bandwidths of actuators

Actuators	Bandwidth, rad/s	Rate limit, deg/s	Position limit, deg
Ailerons δ_a	20.2	80	±21.5
Elevators δ_e	20.2	90	±25
Rudder δ_r	20.2	120	±30

numerically. The nominal aerodynamic model, thrust model, and inertia model are set up adopting the public data of F-16 [49]. The nonlinear dynamic equations of motion before and after failures are given by Eqs. (41) and (45), respectively. The aerodynamic model and control effectiveness after faults/damage are modeled using the methods in Secs. IV.B and IV.C. Only the rudder, ailerons, and stabilizer are considered as inner-loop control variables, and they are all modeled as first-order systems with rate and position limits. The bandwidth and limits for the actuators are listed in Table 2. A simple proportional–integral thrust control to maintain the airspeed is designed in a separate control loop. This aircraft is initially trimmed at a steady-level flight condition with airspeed $V = 500$ ft/s and altitude $h = 10{,}000$ ft. The sampling frequency used by the controllers is $f_s = 100$ Hz.

A.   Flight Control in the Nominal Case

The properties of actuators influence the performance of INDI and (higher-order) sliding-mode control because both methods need "fast" actuator dynamics. The actuator dynamics are included in some (higher-order) sliding-mode controllers [6,26], which would however increase the relative degree of the overall system. This increase would require higher-order derivatives of the outputs, as mentioned in [9]. When the bandwidth of the actuators is sufficiently higher than the system dynamics, the controller can be designed without considering the actuator dynamics, which is a common practice in the literature. This approach is adopted in the present paper, and the control performance is expected to be improved if faster actuators are used.

The successive tracking references for ϕ, θ, ψ are illustrated in Fig. 2, which are smoothly combined sigmoid functions. The sigmoid function $f_r(t) = 1/(1 + e^{-t})$ is chosen because of its differentiable property up to any order.

Remark 8: As discussed in Sec. III.E, NDI-SMC or INDI-SMC actually indicates a branch of sliding-mode control methods designed using the structure of NDI or INDI, regardless of the sliding order, sliding surface, and reaching law designs. Therefore, the comparisons are also independent of these factors. Equations (27) and (28) with first-order integral-type sliding variable [Eq. (24)] are implemented as an example.

The reference tracking controllers using NDI and INDI methods are givens by Eqs. (6) and (10). For fair comparisons, $\boldsymbol{\nu}_c =$

$-\boldsymbol{K}e + \boldsymbol{y}_r^{(\rho)}$ for all the four controllers, with the desired error dynamics consistently given by

$$\ddot{e}_i + K_{D,i}\dot{e}_i + K_{P,i}e_i = 0, \qquad i = 1, 2, 3 \qquad (51)$$

The gains are designed as $K_{D,i} = 5.6$, $K_{P,i} = 16$, $i = 1, 2, 3$ to achieve desired second-order error dynamics with natural frequency 4 rad/s and damping ratio 0.7. $\boldsymbol{\nu}_s$ is designed in the classical way as $\boldsymbol{\nu}_s = -\boldsymbol{K}_s \text{sign}(\boldsymbol{\sigma})$ with $\boldsymbol{K}_s = \text{diag}([1, 0.5, 0.3])$. The widely used boundary-layer method [2,4,6,9,16,25] that replaces the signum functions by saturation functions are also adopted to reduce chattering. The thickness of the boundary layers is $\zeta_i = 0.01$, $i = 1, 2, 3$.

In the nominal condition, namely $\boldsymbol{f} = \bar{\boldsymbol{f}}$, $\boldsymbol{G} = \bar{\boldsymbol{G}}$, the aircraft responses, tracking errors, and control inputs using the proposed four controllers are illustrated in Fig. 3.

As can be seen from Fig. 3, all the four controllers are able to make the system track the commands. Owing to the singular perturbations from the actuator dynamics [16,38], the closed-loop dynamics no long behave like second-order systems under NDI and INDI controls. The aircraft using INDI control has slightly better performance compared to that using NDI, as can be seen from the tracking error responses. Furthermore, by using both NDI and INDI based sliding-mode controllers, the tracking performance is improved without requiring additional control efforts.

B.   Flight Control in the Presence of Actuator Faults

In this subsection, the performance of aircraft command tracking in the presence of actuator faults is simulated. The first actuator fault scenario considered is that the rudder suddenly lost 50% of its effectiveness during flight at $t = 7$ s. As can be seen from Fig. 4, the rotational and directional tracking performance get noticeably worse from $t = 7$ s under the control of NDI, INDI, and NDI-SMC. The tracking errors under NDI control have the largest rms value. Although the aircraft using NDI-SMC is able to recover from the fault, it presents distinct tracking errors during $t \in [7, 13]$ s. On the other hand, INDI-SMC is able to rapidly recover from the rudder fault with much smaller transition tracking errors.

The second actuator fault scenario considered is $t = 3$ s; the right aileron runs away with its maximum rate and gets jammed at $\delta_{a\Delta} = 15.05°$. The positive deflections are defined in the conventional way, namely, a positive δ_a indicates that the right aileron deflects downward and the left aileron deflects upward. As discussed in Sec. IV.B, one side of ailerons stuck at a nonneutral position leads to halved control effectiveness, newly introduced $C_{m_{\delta_a}}$, and aerodynamic coefficient increments given by Eq. (43). As shown in Fig. 5, the aileron jamming induced rolling coefficient ΔC_l makes the aircraft roll to the left from $t = 3$ s under NDI and NDI-SMC control. The coupling effects also make the aircraft yaw to the left under NDI control. ΔC_m makes the aircraft slightly pitch down. NDI control itself shows poor robust performance in this scenario. When combined with sliding-mode control, NDI-SMC has improved robustness, especially on pitch and yaw channels. However, after fault occurs, the aircraft using NDI-SMC is unable to track the rolling command anymore, and the rudder has a potential to get saturated.

On the contrary, aircraft using both INDI and INDI-SMC are able to recover from the aileron fault and continue to track the commands. In view of Fig. 5, the left aileron deflects downward at -14 deg, and the rudder deflects at -2.6 deg after the commands vanish to re-trim the aircraft. Although the aircraft under INDI control can recover, its ϕ tracking performance degrades. When using the INDI control, the rms value of e_ϕ is 0.17 deg in the nominal case, but it degrades to 0.57 deg in the presence of fault. By using INDI-SMC, the rms value of e_ϕ is reduced to 0.07 deg. The aircraft under INDI-SMC also shows better tracking performance in pitch and yaw control channels.

The third actuator fault scenario considered in this paper is the elevator/stabilator jamming problem. At $t = 5$ s, the left stabilator is jammed downward at $\delta_{e\Delta} = -12.5°$. Consequently, the stabilator control effectiveness is halved, $C_{l_{\delta_e}}$, $C_{n_{\delta_e}}$ are introduced, and the
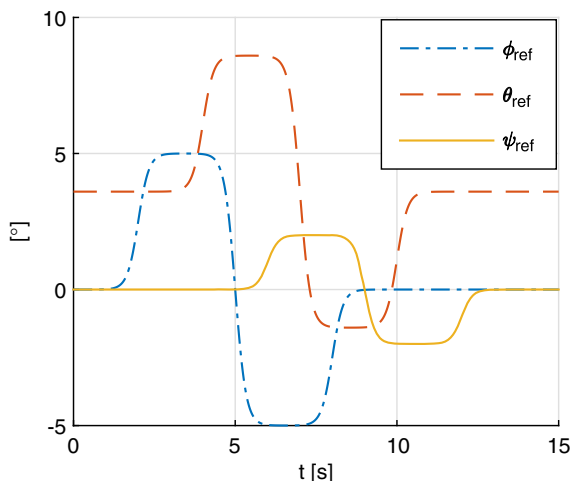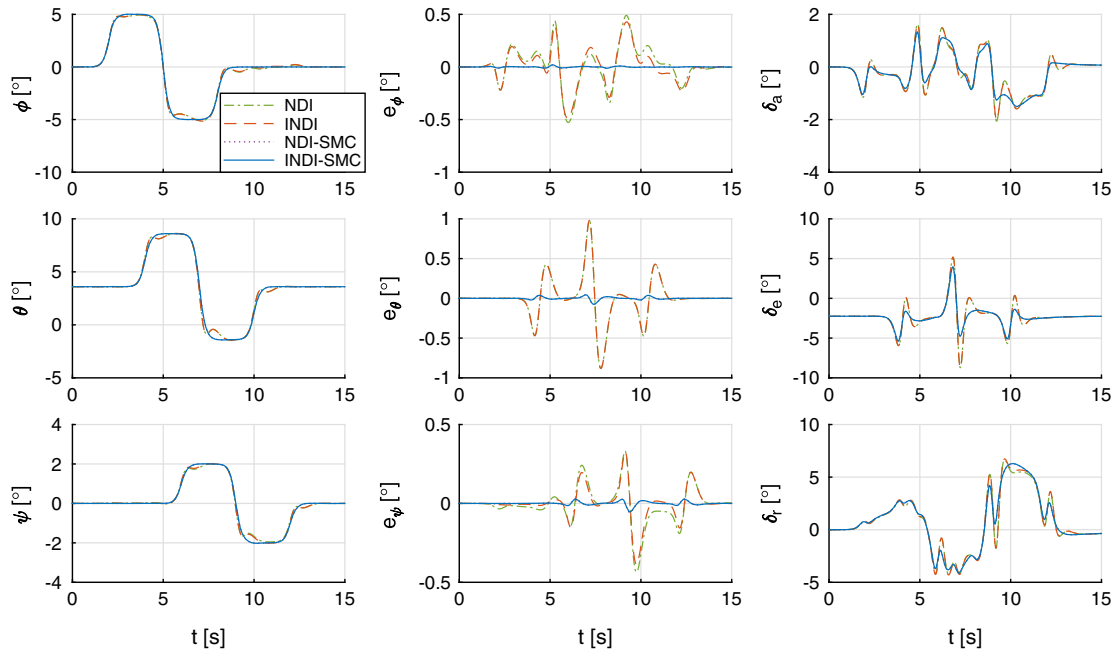

Fig. 2   Tracking commands.

Fig. 3 Aircraft responses and control inputs under the nominal condition.
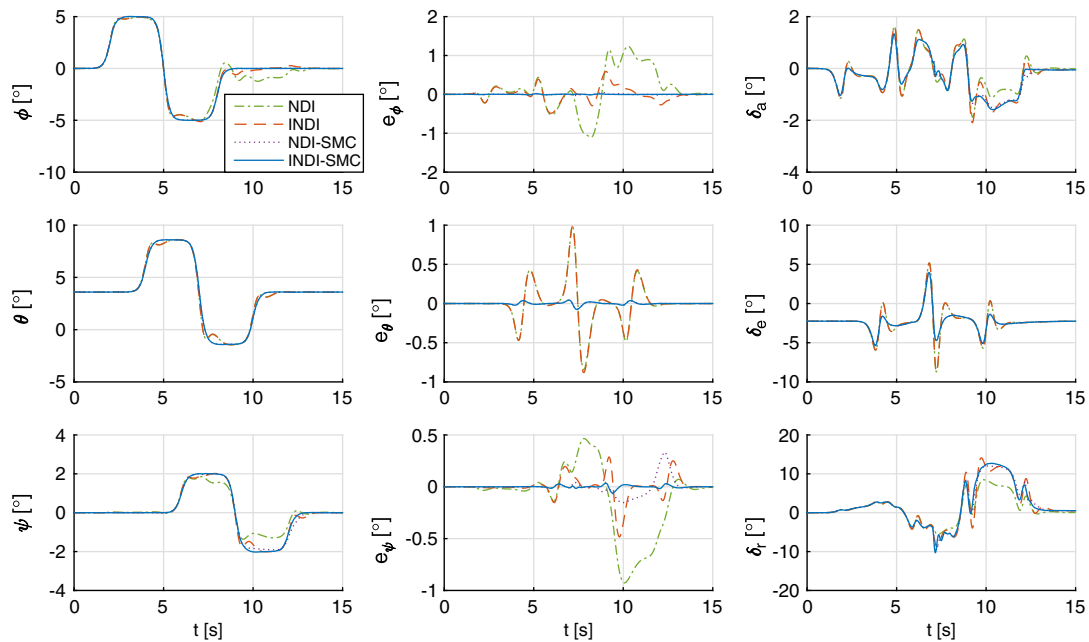

Fig. 4 Aircraft responses and control inputs under a rudder fault condition ($t = 7$ s).

aerodynamic coefficient increments are given by Eq. (44). Theses coefficient increments cause a positive rolling moment and a negative pitching moment, as can be seen from the responses under NDI control in Fig. 6.

Because of the coupling effects, the yaw angle track performance also deteriorates under NDI control. Even though this deterioration is compensated by NDI-SMC, the roll and pitch angles are still unable to recover from the fault under NDI-SMC control. An aircraft using INDI or INDI-SMC is able to recover from the fault and continue to track the commands. Moreover, the rms of e_θ is diminished from 0.29 deg under INDI control to 0.02 deg under INDI-SMC control.

The fourth actuator fault scenario is the combination of the preceding three scenarios with responses shown in Fig. 7. Similar phenomena can be observed that NDI and NDI-SMC are unable to recover from the actuator faults, with the yaw angle showing a trend of divergence. Aircraft using INDI or INDI-SMC can recover and continue to track the commands. However, using INDI control, the

stabilator gets saturated when $t \in [7.1, 7.4]$ s. By contrast, INDI-SMC shows the highest tracking accuracy before and after faults without actuator saturation.

As analyzed in Sec. II.C, the sensor-based INDI control has reduced residual error in the presence of faults/damage as compared to NDI control. Moreover, $\varepsilon_{\text{indi}}$ is guaranteed to be bounded using sufficiently high sampling frequency and if $\|I - \mathcal{B}\bar{\mathcal{B}}^{-1}\| \leq \bar{b} < 1$. On the other hand, the boundedness of ε_{ndi} is undetermined even if $\|I - \mathcal{B}\bar{\mathcal{B}}^{-1}\| \leq \bar{b} < 1$. These phenomena are verified via simulations under the fourth actuator fault scenario as shown in Fig. 8.

As can be observed from Fig. 8, the value of $\|I - \mathcal{B}\bar{\mathcal{B}}^{-1}\|$ for both NDI and INDI show jumps at $t = 3, 5, 7$ s due to successive actuator faults. The variations of $\|I - \mathcal{B}\bar{\mathcal{B}}^{-1}\|$ are because $\mathcal{B}(x)$ is a function of states. $\|I - \mathcal{B}\bar{\mathcal{B}}^{-1}\| \leq \bar{b} < 1$ are satisfied for both NDI and INDI during the entire time history. The residual errors of INDI remain bounded for all the three control channels, whereas $\varepsilon_{\text{ndi},r}$ under NDI control shows a trend of divergence. Furthermore, $\|\varepsilon_{\text{indi}}\|$ is smaller
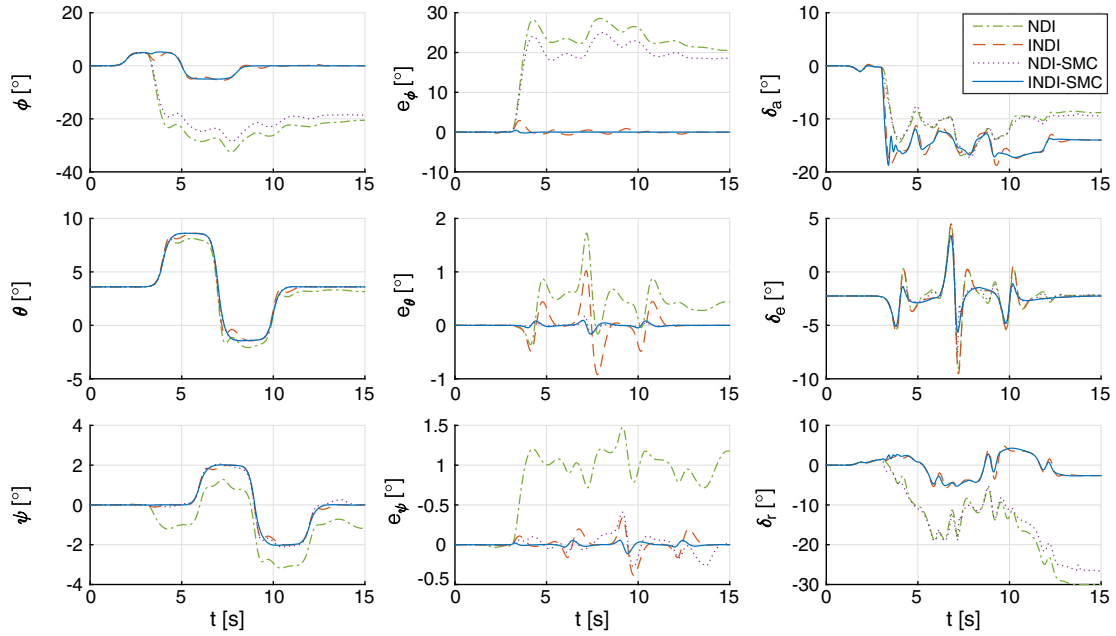
Fig. 5 Aircraft responses and control inputs under an aileron jamming condition ($t = 3$ s).
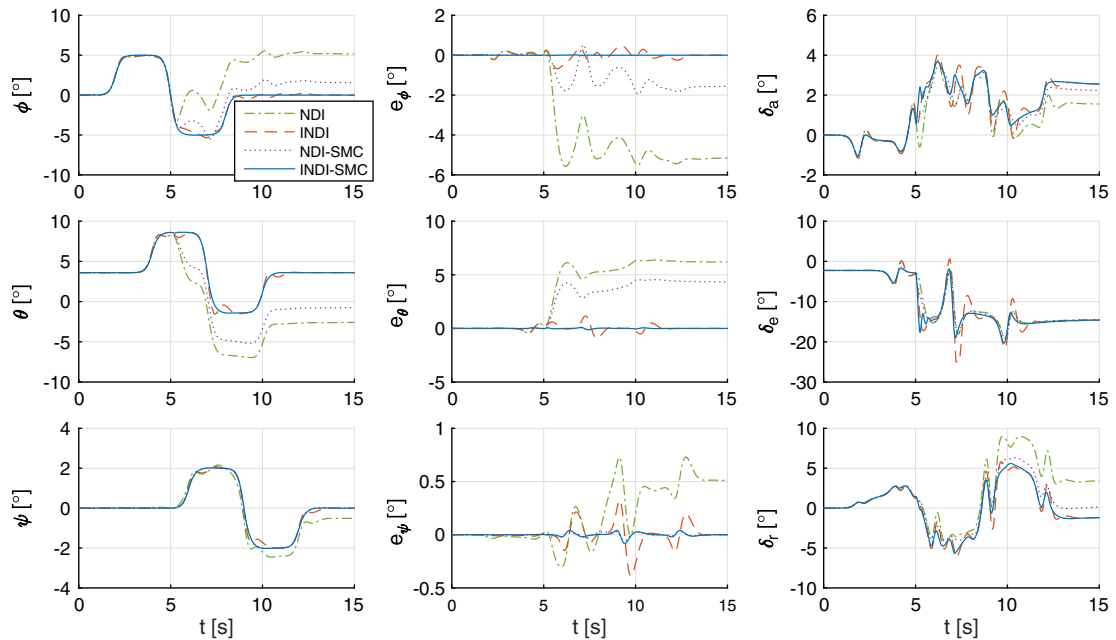

Fig. 6 Aircraft responses and control inputs under a stabilator jamming condition ($t = 5$ s).

than $\|\boldsymbol{\varepsilon}_{\mathrm{ndi}}\|$ in this scenario. It is noteworthy that $\|\boldsymbol{\varepsilon}_{\mathrm{indi}}\|$ can be further diminished by decreasing Δt in practice, whereas $\|\boldsymbol{\varepsilon}_{\mathrm{ndi}}\|$ is independent of Δt.

For the reason that the switching gains of most sliding-mode control methods are monotonically increasing functions of perturbation bounds, the smaller and bounded $\boldsymbol{\varepsilon}_{\mathrm{indi}}$ also requires lower control gains. When the same control gains are used for INDI-SMC and NDI-SMC, which is the situation for all the preceding simulations, INDI-SMC shows better performance. One may suppose that improved performance for NDI-SMC can be achieved if the switching gains are increased. This guess is tested by gradually increasing the switching gains of NDI-SMC as $\boldsymbol{K}_s = c \cdot \mathrm{diag}([1, 0.5, 0.3])$ under the fourth actuator fault scenario, with the simulation results shown in Fig. 9.

In view of Fig. 9, when the switching gains for NDI-SMC increased from $c = 1$ to $c = 5$, the tracking performance of NDI-SMC is indeed improved. However, the roll angle still has about

10 deg of transition error when $c = 5$. Further increasing the gains to $c = 7$ induces a divergence, owing to the rate and position constrains and limited bandwidth of the actuators. The increased switching gains after faults/damage would also amplify the measurement noise in practice. By contrast, the INDI-SMC is able to handle all the considered four actuator fault cases with fixed and lower gains.

C. Flight Control in the Presence of Structural Damage

The aircraft attitude tracking using the proposed four control methods subject to structural damage is simulated in this subsection. The dynamic equations after damage are given by Eq. (45). The aerodynamic effects of damage are given in Sec. IV.C. The inertia properties of this aircraft after damage are calculated by using a Dassault CATIA model of an F-16. Along with the specific component breaks, the corresponding control surface is also damaged. Only the nominal model is known by the controllers, and the faults/damage are intended to be tolerated by the controllers.
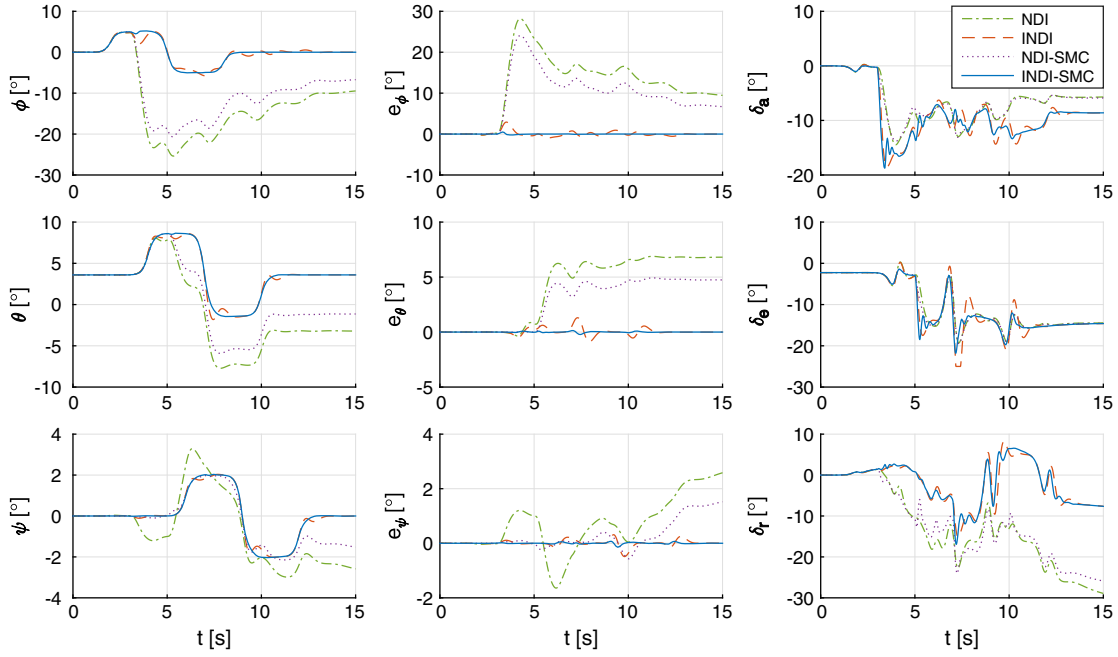
Fig. 7 Aircraft responses and inputs with aileron, stabilator, and rudder faults occur at $t = 3, 5, 7$ s.
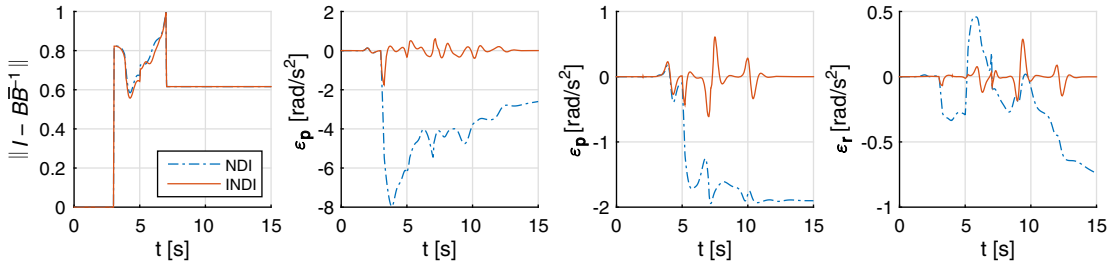

Fig. 8 Value of $\| I - \mathcal{B}\bar{\mathcal{B}}^{-1} \|$ and the residual errors in the fourth actuator fault scenario.
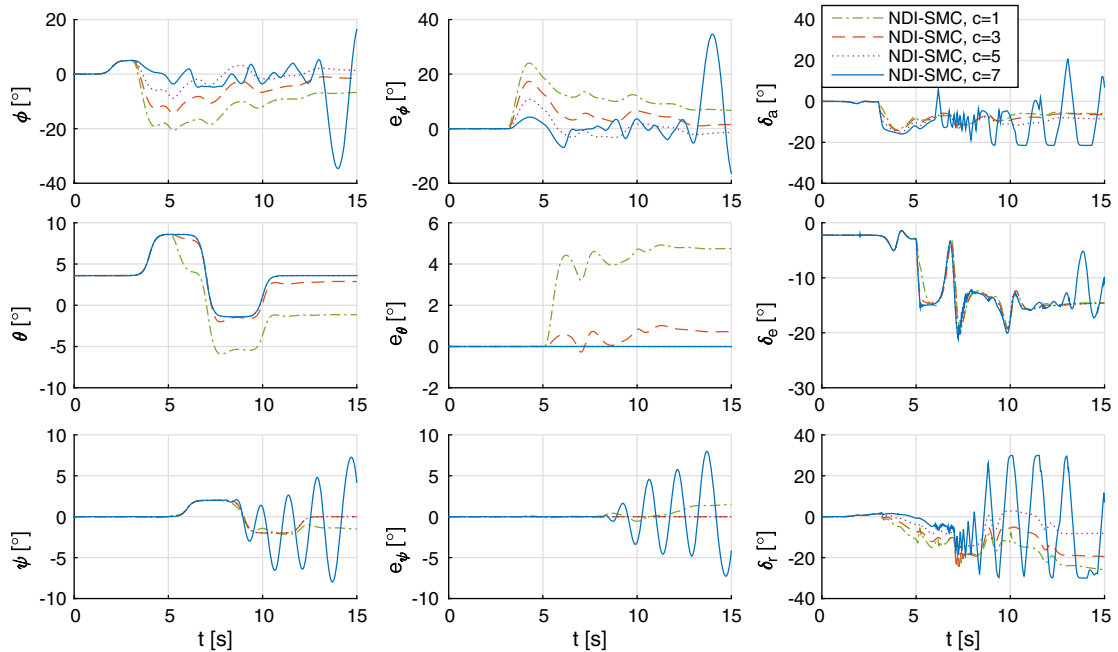

Fig. 9 Responses using NDI-SMC with gradually increased switching gains.

The first structural damage scenario considered here is the vertical tail damage case. To be specific, half of the vertical tail area is lost at $t = 7$ s. At the same time, 50% of the rudder effectiveness is also lost. The system responses and control inputs are presented in Fig. 10.

Figure 10 seems to be similar to Fig. 4 at first glance, but the influences of the forward c.m. shift caused by the vertical tail loss can be seen from the pitch angle tracking error in Fig. 10. Under NDI control, the pitch tracking has a steady-state error of 0.21 deg. The yaw and roll channels also show obvious transition errors under NDI control. NDI-SMC is able to compensate for the errors in roll and pitch channel but still shows noticeable e_ψ. INDI-SMC has improved performance as compared to both INDI and NDI-SMC.

The second structural damage scenario simulated here is that at $t = 5$ s; the entire left stabilator is lost, whereas the right stabilator is still working normally. Accompanying the left stabilator being lost, the c.m. shifts forward and to the right. The effects of the rolling and pitching moment increments can be seen from the responses under NDI control in Fig. 11. The reduced longitudinal damping and stability margin are also influencing the closed-loop system responses. Using NDI control is not enough to make the system recover from this failure. Although NDI-SMC shows improved performance, its convergence speed is slow and still presents small e_θ at $t = 15$ s. Owing to the asymmetrical c.m. shift and the newly induced coefficient ΔC_{l_q}, the rms value of e_ϕ increased to 0.18 deg under INDI control and is reduced by 96% using INDI-SMC.

The third structural damage scenario modeled here is at $t = 3$ s; the right wing lost 25% of its area. At the meanwhile, the right aileron is also lost. The unequal lift on the left and right wing immediately causes a positive rolling moment, as can be seen from Fig. 12. The
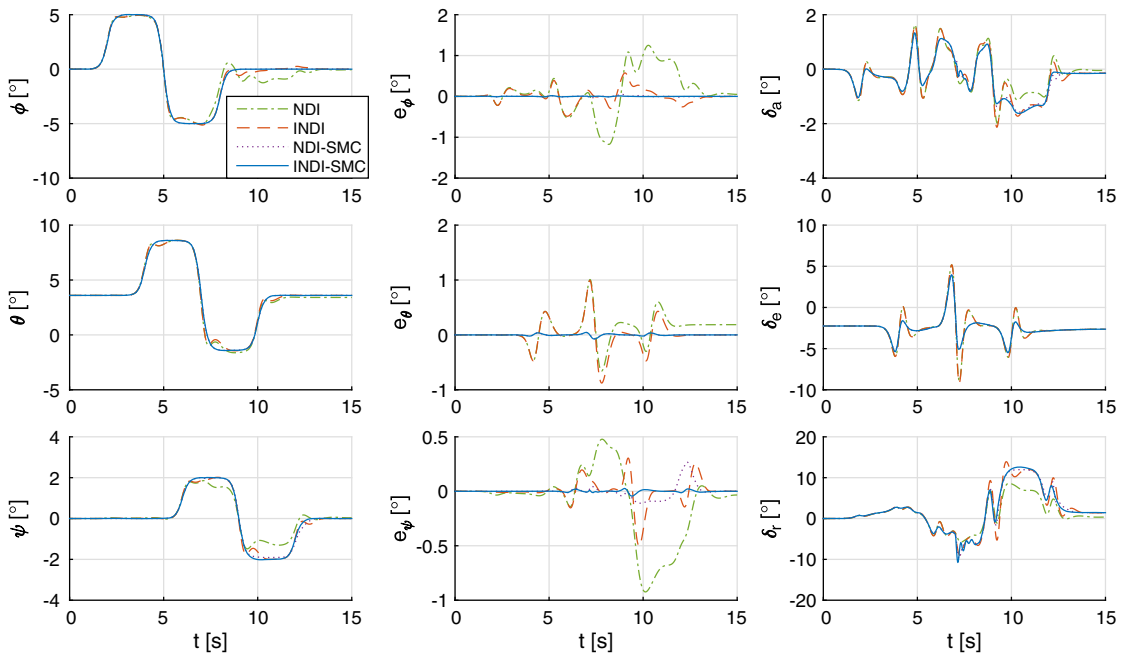

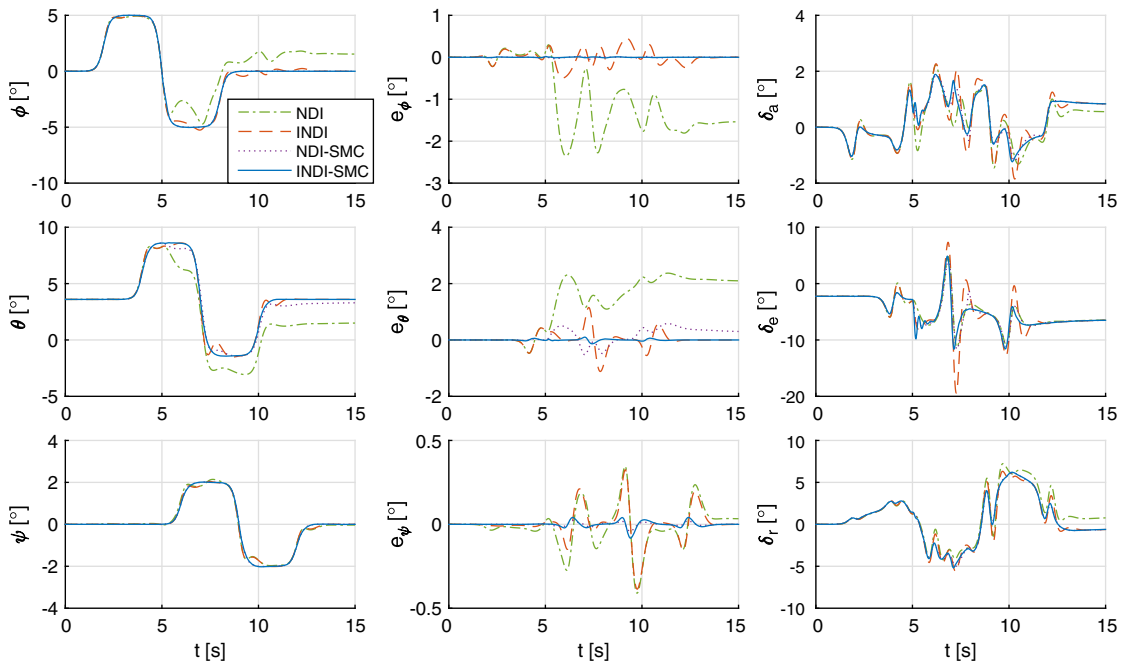**Fig. 10   Aircraft responses and control inputs under a vertical tail damage condition ($t = 7$ s).**

Fig. 11   Aircraft responses and control inputs under a stabilator damage condition ($t = 5$ s).
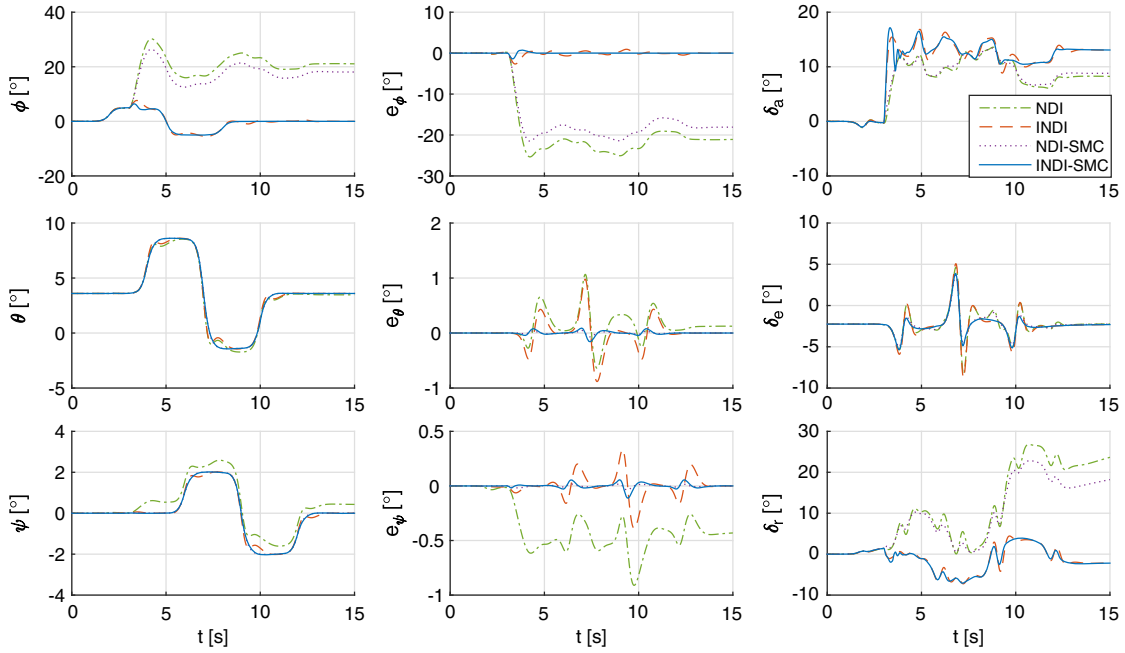
Fig. 12   Aircraft responses and control inputs under a wing damage condition ($t = 3$ s).

coupling effects also cause performance degradations on pitch and yaw channels under NDI and NDI-SMC controls. Using NDI or NDI-SMC, the aircraft is unable to recover from the damage, and the rudder has the potential to get saturated. Both INDI and INDI-SMC are able to make the aircraft recover and continue the tracking missions. The rms value of e_ϕ degrades to 0.51 deg under INDI control in this scenario and can be improved into 0.24 deg using INDI-SMC.

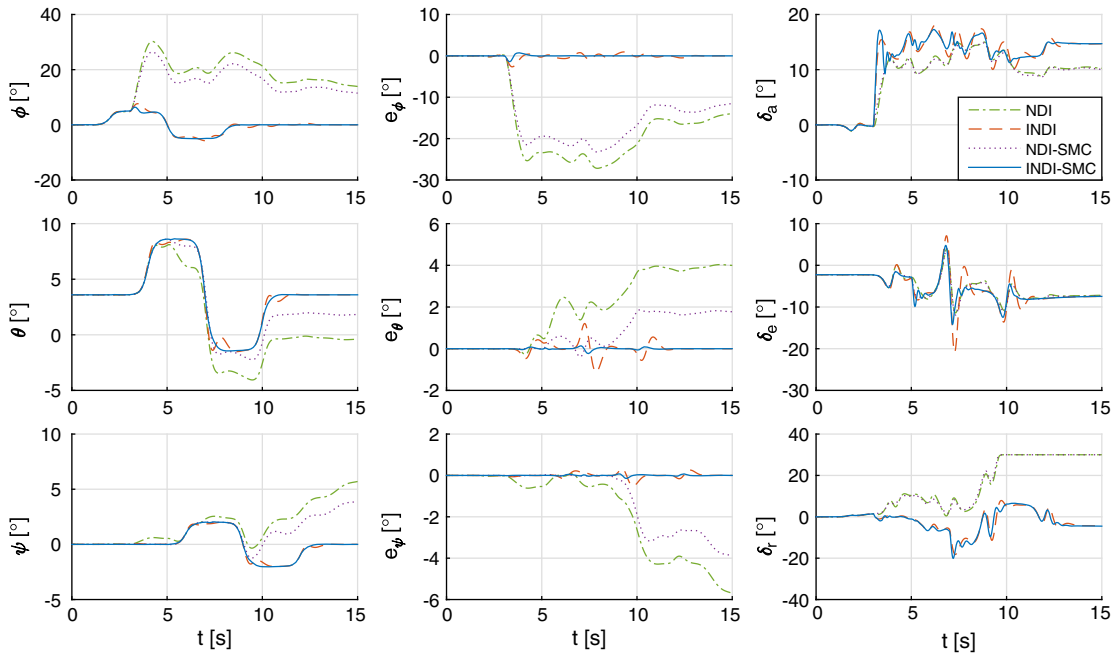**Fig. 13   Aircraft responses and inputs with wing, stabilator, and vertical tail damaged at $t = 3, 5, 7$ s.**
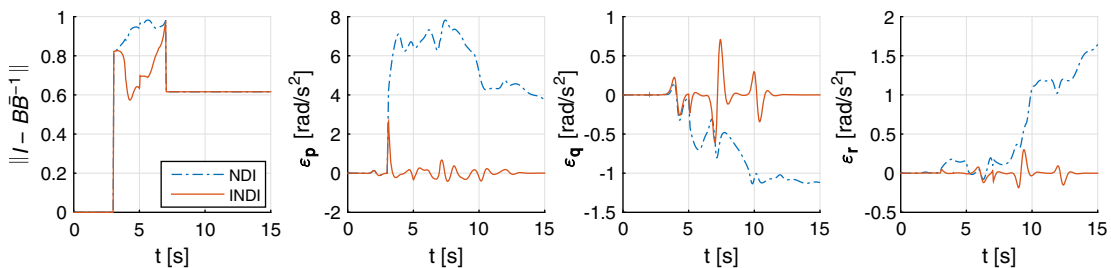

Fig. 14   Value of $\| I - \mathcal{B}\bar{\mathcal{B}}^{-1} \|$ and the residual errors in the fourth structural damage scenario.

The fourth structural damage scenario is a combination of the preceding three structural damage cases. Specifically, 25% of the right wing breaks at $t = 3$ s, the entire left stabilator is lost at $t = 5$ s, and at $t = 7$ s half of the area of the vertical tail is lost. The corresponding control surfaces are also lost along with the structural damage. The simulation results are shown in Fig. 13, from which it can be seen that both NDI and NDI-SMC controls are unable to help the aircraft recover from the damage, and the rudder get saturated from $t = 9.6$ s. INDI as well as INDI-SMC can complete the tracking missions in the presence of structural damage. Furthermore, INDI-SMC has the best tracking accuracy.

Sufficiently high sampling frequency and $\|\boldsymbol{I} - \mathcal{B}\bar{\mathcal{B}}^{-1}\| \leq \bar{b} < 1$ guarantee a bounded $\boldsymbol{\varepsilon}_{\mathrm{indi}}$, whereas the boundedness of $\boldsymbol{\varepsilon}_{\mathrm{ndi}}$ is undetermined under the same conditions (analyses in Sec. II.C). This is also verified when the aircraft is subjected to the fourth damage scenario, as illustrated in Fig. 14, where $\varepsilon_{\mathrm{ndi},r}$ shows a trend of divergence. Furthermore, $\|\boldsymbol{\varepsilon}_{\mathrm{indi}}\|$ is smaller than $\|\boldsymbol{\varepsilon}_{\mathrm{ndi}}\|$ in Fig. 14, which leads to smaller minimum possible gain values for INDI-SMC.

VI. Conclusions

The incremental sliding-mode control (INDI-SMC) framework is proposed in this paper by hybridizing (higher-order) sliding-mode controllers/observers with the reformulated incremental nonlinear dynamic inversion (INDI). The incorporations of the sliding mode robustification terms into INDI compensate for the residual errors of INDI, whereas the incremental framework simultaneously reduces the minimum possible control/observer gains and the model dependency.

It is verified theoretically and numerically that a diagonally dominant structure of $\mathcal{B}\bar{\mathcal{B}}^{-1}$ and sufficiently high sampling frequency ensure the boundedness of the INDI residual error ($\boldsymbol{\varepsilon}_{\mathrm{indi}}$). By contrast, even if these conditions are satisfied, the nonlinear dynamic inversion (NDI) residual error ($\boldsymbol{\varepsilon}_{\mathrm{ndi}}$) can become unbounded in severe damage cases. Moreover, in the same faults/damage scenario, there exists a sampling frequency that makes the bound of $\boldsymbol{\varepsilon}_{\mathrm{indi}}$ smaller than the bound of $\boldsymbol{\varepsilon}_{\mathrm{ndi}}$. These beneficial properties of INDI enable the INDI-SMC framework to passively resist a wider range of perturbations with lower sliding-mode control/observer gains, as compared to the widely used way of designing sliding-mode control based on NDI.

When applied to passive fault-tolerant flight control problems, the proposed INDI-SMC framework shows better robust performance over NDI, INDI, and the NDI-based sliding-mode control, in the presence of sudden actuator faults and structural damage, which makes it a promising approach to enhance aircraft survivability in real life.

References

[1] Zhang, Y., and Jiang, J., "Bibliographical Review on Reconfigurable Fault-Tolerant Control Systems," *Annual Reviews in Control*, Vol. 32, No. 2, 2008, pp. 229–252.
doi:10.1016/j.arcontrol.2008.03.008

[2] Kim, D., and Kim, Y., "Robust Variable Structure Controller Design for Fault Tolerant Flight Control," *Journal of Guidance, Control, and Dynamics*, Vol. 23, No. 3, 2000, pp. 430–437.
doi:10.2514/2.4577

[3] Hung, J. Y., Gao, W., and Hung, J. C., "Variable Structure Control: A Survey," *IEEE Transactions on Industrial Electronics*, Vol. 40, No. 1, 1993, pp. 2–22.
doi:10.1109/41.184817

[4] Slotine, J.-J. E., and Li, W., *Applied Nonlinear Control*, Prentice–Hall, Englewood Cliffs, NJ, 1991, pp. 276–301.

[5] Shtessel, Y., Buffington, J., and Banda, S., "Tailless Aircraft Flight Control Using Multiple Time Scale Reconfigurable Sliding Modes," *IEEE Transactions on Control Systems Technology*, Vol. 10, No. 2, 2002, pp. 288–296.
doi:10.1109/87.987075

[6] Shtessel, Y. B., Buffington, J. M., and Banda, S. S., "Multiple Timescale Flight Control Using Reconfigurable Sliding Modes," *Journal of Guidance, Control, and Dynamics*, Vol. 22, No. 6, 1999, pp. 873–883.
doi:10.2514/2.4465

[7] Alwi, H., and Edwards, C., "Fault Tolerant Control Using Sliding Modes with On-Line Control Allocation," *Automatica*, Vol. 44, No. 7, 2008, pp. 1859–1866.
doi:10.1016/j.automatica.2007.10.034

[8] Alwi, H., "Fault Tolerant Sliding Mode Control Schemes with Aerospace Applications," Ph.D. Thesis, Univ. of Leicester, Leicester, England, U.K., 2008.

[9] Hess, R. A., and Wells, S. R., "Sliding Mode Control Applied to Reconfigurable Flight Control Design," *Journal of Guidance, Control, and Dynamics*, Vol. 26, No. 3, 2003, pp. 452–462.
doi:10.2514/2.5083

[10] Wang, T., Xie, W., and Zhang, Y., "Sliding Mode Fault Tolerant Control Dealing with Modeling Uncertainties and Actuator Faults," *ISA Transactions*, Vol. 51, No. 3, 2012, pp. 386–392.
doi:10.1016/j.isatra.2012.02.003

[11] Hamayun, M. T., Edwards, C., and Alwi, H., "A Fault Tolerant Control Allocation Scheme with Output Integral Sliding Modes," *Automatica*, Vol. 49, No. 6, 2013, pp. 1830–1837.
doi:10.1016/j.automatica.2013.02.043

[12] Chen, L., Alwi, H., Edwards, C., and Sato, M., "Flight Evaluation of an LPV Sliding Mode Controller with Online Control Allocation," *Proceedings of the 56th IEEE Annual Conference on Decision and Control*, IEEE Publ., Piscataway, NJ, 2017, pp. 3928–3933.
doi:10.1109/CDC.2017.8264237

[13] Utkin, V. I., and Poznyak, A. S., "Adaptive Sliding Mode Control with Application to Super-Twist Algorithm: Equivalent Control Method," *Automatica*, Vol. 49, No. 1, 2013, pp. 39–47.
doi:10.1016/j.automatica.2012.09.008

[14] Edwards, C., and Shtessel, Y. B., "Adaptive Continuous Higher Order Sliding Mode Control," *Automatica*, Vol. 65, March 2016, pp. 183–190.
doi:10.1016/j.automatica.2015.11.038

[15] Edwards, C., and Shtessel, Y. B., "Continuous Higher Order Sliding Mode Control Based on Adaptive Disturbance Compensation," *Proceedings of the 13th International Workshop on Variable Structure Systems*, Vol. 47, IEEE Publ., Piscataway, NJ, 2014, pp. 1–5.
doi:10.1109/VSS.2014.6881147

[16] Khalil, H. K., *Nonlinear Systems*, Prentice–Hall, Englewood Cliffs, NJ, 2002, pp. 515–517, 552–578.

[17] Edwards, C., and Shtessel, Y., "Adaptive Dual-Layer Super-Twisting Control and Observation," *International Journal of Control*, Vol. 89, No. 9, 2016, pp. 1759–1766.
doi:10.1080/00207179.2016.1175030

[18] Massey, T. E., and Shtessel, Y. B., "Continuous Traditional and High-Order Sliding Modes for Satellite Formation Control," *Journal of Guidance, Control, and Dynamics*, Vol. 28, No. 4, 2005, pp. 826–831.
doi:10.2514/1.14126

[19] Hall, C. E., and Shtessel, Y. B., "Sliding Mode Disturbance Observer-Based Control for a Reusable Launch Vehicle," *Journal of Guidance, Control, and Dynamics*, Vol. 29, No. 6, 2006, pp. 1315–1328.
doi:10.2514/1.20151

[20] Besnard, L., Shtessel, Y. B., and Landrum, B., "Quadrotor Vehicle Control via Sliding Mode Controller Driven by Sliding Mode Disturbance Observer," *Journal of the Franklin Institute*, Vol. 349, No. 2, 2012, pp. 658–684.
doi:10.1016/j.jfranklin.2011.06.031

[21] Orr, J. S., and Shtessel, Y. B., "Lunar Spacecraft Powered Descent Control Using Higher-Order Sliding Mode Techniques," *Journal of the Franklin Institute*, Vol. 349, No. 2, 2012, pp. 476–492.
doi:10.1016/j.jfranklin.2011.06.015

[22] Sieberling, S., Chu, Q. P., and Mulder, J. A., "Robust Flight Control Using Incremental Nonlinear Dynamic Inversion and Angular Acceleration Prediction," *Journal of Guidance, Control, and Dynamics*, Vol. 33, No. 6, 2010, pp. 1732–1742.
doi:10.2514/1.49978

[23] Simplício, P., Pavel, M., van Kampen, E., and Chu, Q., "An Acceleration Measurements-Based Approach for Helicopter Nonlinear Flight Control Using Incremental Nonlinear Dynamic Inversion," *Control Engineering Practice*, Vol. 21, No. 8, 2013, pp. 1065–1077.
doi:10.1016/j.conengprac.2013.03.009

[24] Lu, P., van Kampen, E., de Visser, C., and Chu, Q., "Aircraft Fault-Tolerant Trajectory Control Using Incremental Nonlinear Dynamic Inversion," *Control Engineering Practice*, Vol. 57, Dec. 2016, pp. 126–141.
doi:10.1016/j.conengprac.2016.09.010

[25] Shtessel, Y., Hall, C., and Jackson, M., "Reusable Launch Vehicle Control in Multiple-Time-Scale Sliding Modes," *Journal of Guidance, Control, and Dynamics*, Vol. 23, No. 6, 2000, pp. 1013–1020.
doi:10.2514/2.4669

[26] Shtessel, Y. B., and Shkolnikov, I. A., "Aeronautical and Space Vehicle Control in Dynamic Sliding Manifolds," *International Journal of Control*, Vol. 76, Nos. 9–10, 2003, pp. 1000–1017.
doi:10.1080/0020717031000099065

[27] Feng, Y., Yu, X., and Man, Z., "Non-Singular Terminal Sliding Mode Control of Rigid Manipulators," *Automatica*, Vol. 38, No. 12, 2002, pp. 2159–2167.
doi:10.1016/S0005-1098(02)00147-4

[28] Wu, Y., Yu, X., and Man, Z., "Terminal Sliding Mode Control Design for Uncertain Dynamic Systems," *Systems & Control Letters*, Vol. 34, No. 5, 1998, pp. 281–287.
doi:10.1016/S0167-6911(98)00036-X

[29] Yu, S., Yu, X., Shirinzadeh, B., and Man, Z., "Continuous Finite-Time Control for Robotic Manipulators with Terminal Sliding Mode," *Automatica*, Vol. 41, No. 11, 2005, pp. 1957–1964.
doi:10.1016/j.automatica.2005.07.001

[30] Defoort, M., Floquet, T., Kokosy, A., and Perruquetti, W., "A Novel Higher Order Sliding Mode Control Scheme," *Systems and Control Letters*, Vol. 58, No. 2, 2009, pp. 102–108.
doi:10.1016/j.sysconle.2008.09.004

[31] Sagliano, M., Mooij, E., and Theil, S., "Adaptive Disturbance-Based High-Order Sliding-Mode Control for Hypersonic-Entry Vehicles," *Journal of Guidance, Control, and Dynamics*, Vol. 40, No. 3, 2017, pp. 521–536.
doi:10.2514/1.G000675

[32] Wang, J., Zong, Q., Su, R., and Tian, B., "Continuous High Order Sliding Mode Controller Design for a Flexible Air-Breathing Hypersonic Vehicle," *ISA Transactions*, Vol. 53, No. 3, 2014, pp. 690–698.
doi:10.1016/j.isatra.2014.01.002

[33] Yu, P., Shtessel, Y., and Edwards, C., "Continuous Higher Order Sliding Mode Control with Adaptation of Air Breathing Hypersonic Missile," *International Journal of Adaptive Control and Signal Processing*, Vol. 30, Nos. 8–10, 2016, pp. 1099–1117.
doi:10.1002/acs.v30.8-10

[34] Acquatella, P., Falkena, W., van Kampen, E., and Chu, Q. P., "Robust Nonlinear Spacecraft Attitude Control using Incremental Nonlinear Dynamic Inversion," *AIAA Guidance, Navigation, and Control Conference*, AIAA Paper 2012-4623, Aug. 2012, pp. 1–20.
doi:10.2514/6.2012-4623

[35] Wang, X., Van Kampen, E., and Chu, Q. P., "Gust Load Alleviation and Ride Quality Improvement with Incremental Nonlinear Dynamic Inversion," *AIAA Atmospheric Flight Mechanics Conference*, AIAA Paper 2017-1400, 2017.
doi:10.2514/6.2017-1400

[36] Smeur, E. J. J., Chu, Q. P., and de Croon, G. C. H. E., "Adaptive Incremental Nonlinear Dynamic Inversion for Attitude Control of Micro Air Vehicles," *Journal of Guidance, Control, and Dynamics*, Vol. 39, No. 3, 2016, pp. 450–461.
doi:10.2514/1.G001490

[37] Grondman, F., Looye, G., Kuchar, R. O., Chu, Q. P., and Van Kampen, E., "Design and Flight Testing of Incremental Nonlinear Dynamic Inversion-Based Control Laws for a Passenger Aircraft," *2018 AIAA Guidance, Navigation, and Control Conference*, AIAA Paper 2018-0385, 2018.
doi:10.2514/6.2018-0385

[38] Wang, X., Van Kampen, E., Chu, Q. P., and Lu, P., "Stability Analysis for Incremental Nonlinear Dynamic Inversion Control," *20180 AIAA Guidance, Navigation, and Control Conference*, AIAA Paper 2018-1115, 2018.
doi:10.2514/6.2018-1115

[39] Marzat, J., Piet-Lahanier, H., Damongeot, F., and Walter, E., "Model-Based Fault Diagnosis for Aerospace Systems: A Survey," *Proceedings of the Institution of Mechanical Engineers, Part G: Journal of Aerospace Engineering*, Vol. 226, No. 10, 2012, pp. 1329–1360.
doi:10.1177/0954410011421717

[40] Levant, A., "Higher-Order Sliding Modes, Differentiation and Output-Feedback Control," *International Journal of Control*, Vol. 76, Nos. 9–10, 2003, pp. 924–941.
doi:10.1080/0020717031000099029

[41] Utkin, V., Guldner, J., and Shi, J., *Sliding Mode Control in Electro-Mechanical Systems*, 2nd ed., Automation and Control Engineering, Vol. 31, CRC Press, London, 2009, pp. 28–33.
doi:10.1201/9781420065619

[42] Laghrouche, S., Plestan, F., and Glumineau, A., "Higher Order Sliding Mode Control Based on Integral Sliding Mode," *Automatica*, Vol. 43, No. 3, 2007, pp. 531–537.
doi:10.1016/j.automatica.2006.09.017

[43] Levant, A., "Sliding Order and Sliding Accuracy in Sliding Mode Control," *International Journal of Control*, Vol. 58, No. 6, 1993, pp. 1247–1263.
doi:10.1080/00207179308923053

[44] Filippov, A. F., *Differential Equations with Discontinuous Righthand Sides*, Mathematics and Its Applications, Vol. 18, Springer, Dordrecht, The Netherlands, 1988, pp. 115–126.
doi:10.1007/978-94-015-7793-9

[45] Bhat, S. P., and Bernstein, D. S., "Geometric Homogeneity with Applications to Finite-Time Stability," *Mathematics of Control, Signals, and Systems*, Vol. 17, No. 2, 2005, pp. 101–127.
doi:10.1007/s00498-005-0151-x

[46] Shah, G., "Aerodynamic Effects and Modeling of Damage to Transport Aircraft," *AIAA Atmospheric Flight Mechanics Conference and Exhibit*, AIAA Paper 2008-6203, Aug. 2008.
doi:10.2514/6.2008-6203

[47] Bacon, B., and Gregory, I., "General Equations of Motion for a Damaged Asymmetric Aircraft," *AIAA Atmospheric Flight Mechanics Conference and Exhibit*, AIAA Paper 2007-6306, Aug. 2007.
doi:10.2514/6.2007-6306

[48] Zhang, Y., de Visser, C. C., and Chu, Q. P., "Aircraft Damage Identification and Classification for Database-Driven Online Flight-Envelope Prediction," *Journal of Guidance, Control, and Dynamics*, Vol. 41, No. 2, 2017, pp. 1–12.
doi:10.2514/1.G002866

[49] Nguyen, L. T., Ogburn, M. E., Gilbert, W. P., Kibler, K. S., Brown, P. W., and Deal, P. L., "Simulator Study of Stall/Post-Stall Characteristics of a Fighter Airplane with Relaxed Longitudinal Static Stability," NASA TP 1538, 1979.

This article has been cited by:

1. Yongchao Wang, Zengjie Zhang, Cong Li, Martin Buss. 2022. Adaptive incremental sliding mode control for a robot manipulator. *Mechatronics* **82**, 102717. [Crossref]

2. Tuo Han, Qinglei Hu, Hyo-Sang Shin, Antonios Tsourdos, Ming Xin. 2022. Incremental Twisting Fault Tolerant Control for Hypersonic Vehicles With Partial Model Knowledge. *IEEE Transactions on Industrial Informatics* **18**:2, 1050-1060. [Crossref]

3. Jing Chang, Roeland De Breuker, Xuerui Wang. Discrete-time Design and Stability Analysis for Nonlinear Incremental Fault-tolerant Flight Control . [Abstract] [PDF] [PDF Plus]

4. Salahudden Salahudden, Akash T. Das, Dipak K. Giri, Ajoy K. Ghosh. Aircraft Spiral Recovery with Altitude Control . [Abstract] [PDF] [PDF Plus]

5. Paul Acquatella, Erik-Jan Van Kampen, Qi P. Chu. A Sampled-Data Form of Incremental Nonlinear Dynamic Inversion for Spacecraft Attitude Control . [Abstract] [PDF] [PDF Plus]

6. Balaji Jayaraman, Kumar Gaurav, Dipak K. Giri, Ajoy K. Ghosh. Nonsingular Fast Terminal Sliding Mode Flight Control of a Subscale Aircraft . [Abstract] [PDF] [PDF Plus]

7. Beau Smit, Tijmen Pollack, Erik-Jan Van Kampen. Adaptive Incremental Nonlinear Dynamic Inversion Flight Control for Consistent Handling Qualities . [Abstract] [PDF] [PDF Plus]

8. Tijmen Pollack, Erik-Jan Van Kampen. Robust Stability and Performance Analysis of Incremental Dynamic Inversion-based Flight Control Laws . [Abstract] [PDF] [PDF Plus]

9. Salahudden Salahudden, Ajoy K. Ghosh. Robust Control Design, with and without Perturbation, for Aircraft Attitude Control in Flat-Spin Motion . [Abstract] [PDF] [PDF Plus]

10. Renwei Zuo, Yinghui Li, Maolong Lv, Zongcheng Liu, Zehong Dong. 2022. Design of singularity-free fixed-time fault-tolerant control for HFVs with guaranteed asymmetric time-varying flight state constraints. *Aerospace Science and Technology* **120**, 107270. [Crossref]

11. Xuerui Wang, Tigran Mkhoyan, Roeland De Breuker. 2022. Nonlinear Incremental Control for Flexible Aircraft Trajectory Tracking and Load Alleviation. *Journal of Guidance, Control, and Dynamics* **45**:1, 39-57. [Abstract] [Full Text] [PDF] [PDF Plus]

12. Muhammad Sohail Khan Raja, Qasim Ali. 2021. Recent advances in active fault tolerant flight control systems. *Proceedings of the Institution of Mechanical Engineers, Part G: Journal of Aerospace Engineering* **35**, 095441002110628. [Crossref]

13. Tuo Han, Qinglei Hu, Hyo-Sang Shin, Antonios Tsourdos, Ming Xin. 2021. Sensor-Based Robust Incremental Three-Dimensional Guidance Law with Terminal Angle Constraint. *Journal of Guidance, Control, and Dynamics* **44**:11, 2016-2030. [Abstract] [Full Text] [PDF] [PDF Plus]

14. Rafael A. Cordeiro, Jose R. Azinheira, Alexandra Moutinho. 2021. Robustness of Incremental Backstepping Flight Controllers: The Boeing 747 Case Study. *IEEE Transactions on Aerospace and Electronic Systems* **57**:5, 3492-3505. [Crossref]

15. Xuerui Wang, Tigran Mkhoyan, Iren Mkhoyan, Roeland De Breuker. 2021. Seamless Active Morphing Wing Simultaneous Gust and Maneuver Load Alleviation. *Journal of Guidance, Control, and Dynamics* **44**:9, 1649-1662. [Abstract] [Full Text] [PDF] [PDF Plus]

16. Shuaipeng Lang, Fubiao Zhang, Zhiwen Sun. Fault Tolerant Control for a Hexacopter Based on Optimal Adaptive Control Allocation 4397-4402. [Crossref]

17. Moon Gyeang Cho, Useok Jung, Jun-Young An, Yoo-Seung Choi, Chang-Joo Kim. 2021. Adaptive Trajectory Tracking Control for Rotorcraft Using Incremental Backstepping Sliding Mode Control Strategy. *International Journal of Aerospace Engineering* **2021**, 1-15. [Crossref]

18. Salahudden, Vijay S Dwivedi, Prasiddha N Dwivedi, Dipak K Giri, Ajoy K Ghosh. 2021. Aircraft flat-spin recovery using sliding-mode based attitude and altitude control. *Proceedings of the Institution of Mechanical Engineers, Part G: Journal of Aerospace Engineering* **235**:8, 924-936. [Crossref]

19. Bo Sun, Erik-Jan van Kampen. 2021. Intelligent adaptive optimal control using incremental model-based global dual heuristic programming subject to partial observability. *Applied Soft Computing* **103**, 107153. [Crossref]

20. Xuerui Wang, Tigran Mkhoyan, Roeland De Breuker. Nonlinear Incremental Control for Flexible Aircraft Trajectory Tracking and Load Alleviation . [Abstract] [PDF] [PDF Plus]

21. Erwin Mooij, Xuerui Wang. Incremental Sliding Mode Control for Aeroelastic Launch Vehicles with Propellant Slosh . [Abstract] [PDF] [PDF Plus]

22. Liam Vile, Halim Alwi, Christopher Edwards. 2021. Robust fault tolerant control allocation for a modern over-actuated commercial aircraft. *IET Control Theory & Applications* **15**:2, 307-322. [Crossref]

23. Baoxu Jia, Liguo Sun, Yanyang Wang, Xiaoyu Liu, Weigao Dang. 2021. Switched Adaptive Sliding Mode Disturbance Observer for Nonlinear Fault-Tolerant Flight Control. *IEEE Access* **9**, 92614-92628. [Crossref]

24. Yinan Miao, Xingjian Wang, Yiqi Miao, Shaoping Wang. 2020. Dynamics and adaptive fault-tolerant flight control under structure damage of horizontal stabilizer. *Aerospace Science and Technology* **106**, 106135. [Crossref]

25. Davood Asadi, Karim Ahmadi. 2020. Nonlinear robust adaptive control of an airplane with structural damage. *Proceedings of the Institution of Mechanical Engineers, Part G: Journal of Aerospace Engineering* **234**:14, 2076-2088. [Crossref]

26. Liguo SUN, Qing ZHOU, Baoxu JIA, Wenqian TAN, Hangxu LI. 2020. Effective control allocation using hierarchical multi-objective optimization for multi-phase flight. *Chinese Journal of Aeronautics* **33**:7, 2002-2013. [Crossref]

27. Mojtaba Mirzaei, Iman Hosseini, Valiollah Ghaffari. 2020. MEMS gyroscope fault detection and elimination for an underwater robot using the combination of smooth switching and dynamic redundancy method. *Microelectronics Reliability* **109**, 113677. [Crossref]

28. Bo Sun, Erik-Jan van Kampen. 2020. Incremental model-based global dual heuristic programming with explicit analytical calculations applied to flight control. *Engineering Applications of Artificial Intelligence* **89**, 103425. [Crossref]

29. B. Paul Acquatella, Qi Ping Chu. 2020. Agile Spacecraft Attitude Control: an Incremental Nonlinear Dynamic Inversion Approach. *IFAC-PapersOnLine* **53**:2, 5709-5716. [Crossref]

30. Xuerui Wang, Erik-Jan van Kampen, Qiping Chu. 2019. Quadrotor fault-tolerant incremental nonsingular terminal sliding mode control. *Aerospace Science and Technology* **95**, 105514. [Crossref]

31. Xuerui Wang, Erik-Jan van Kampen, Qiping Chu, Peng Lu. 2019. Stability Analysis for Incremental Nonlinear Dynamic Inversion Control. *Journal of Guidance, Control, and Dynamics* **42**:5, 1116-1129. [Abstract] [Full Text] [PDF] [PDF Plus]

32. Xuerui Wang, Sihao Sun, Erik-Jan van Kampen, Qiping Chu. 2019. Quadrotor Fault Tolerant Incremental Sliding Mode Control driven by Sliding Mode Disturbance Observers. *Aerospace Science and Technology* **87**, 417-430. [Crossref]

33. Bo Sun, Erik-Jan van Kampen. 2019. Incremental Model-Based Global Dual Heuristic Programming for Flight Control. *IFAC-PapersOnLine* **52**:29, 7-12. [Crossref]